Simple models for an injection molding system

Article *in* Canadian Applied Mathematics Quarterly · January 2004

CITATIONS
0

READS
555

6 authors, including:

Tim G Myers
CRM Centre for Mathematical Research
128 PUBLICATIONS **2,425** CITATIONS

SEE PROFILE

CANADIAN APPLIED
MATHEMATICS QUARTERLY
Volume 12, Number 4, Winter 2004

SIMPLE MODELS FOR AN INJECTION MOLDING SYSTEM

GREGORY LEWIS,[1] IAN FRIGAARD,[2] HUAXIONG HUANG,[3]
TIM MYERS,[4] REX WESTBROOK[5] AND MARIANA
CARRASCO-TEJA[2]

Based on work carried out at the Eighth Annual Industrial Problem Solving Workshop, sponsored by the Pacific Institute for the Mathematical Sciences, May 17–21, 2004. Original problem submitted by Husky Injection Molding Systems.

ABSTRACT. We develop simple models that can be used to predict the forces of impact that occur during the injection molding process involving a magnesium alloy. We model the impact of the injection molding screw tip on the molten material entering the mold, and the impact of the piston flange on the machine housing, which can occur when the amount of material that has been injected into the mold is insufficient to completely fill the mold. We consider the effects due to the elasticity of the molten material and machine parts, those due to the presence of a thin film of hydraulic fluid between the piston flange and machine housing, the variation of the viscosity of the hydraulic fluid, and those due to the leakage of molten metal past the screw tip.

With the simple models developed here, an injection molding machine designer can predict how varying the process parameters may affect the impact forces, and thus, may be able to more efficiently design the machine so that damage is less likely to occur during operation. This will result a longer life for the machine, which will lead to increased cost effectiveness for the manufacturer.

[1]Faculty of Science, University of Ontario IT, Oshawa, ON
[2]Departments of Mathematics and Mechanical Engineering, University of British Columbia, Vancouver, BC
[3]Department of Mathematics and Statistics, York University, Toronto, ON
[4]Department of Mathematics and Applied Mathematics, University of Cape Town, South Africa
[5]Department of Mathematics and Statistics, University of Calgary, Calgary, AB

1 Introduction Injection molding consists of forcing a melted material into a mold cavity, allowing the material to cool and harden, then ejecting the product from the mold. Injection molding has been used for many years to manufacture a wide range of products, including buttons, plastic drink bottles, and computer mice (see, e.g., Bryce [**2**] for a history and description of the injection molding process and machine). The process is particularly efficient for the mass production of parts that have intricate geometry that would be expensive or difficult to machine or cast.

The most common material used in injection molding are thermoplastics. However, processes have also been developed for the injection molding of metals, such as certain ferrous-based alloys, stainless steels, and copper [**3**]. Recently, a process called thixo-molding that uses a magnesium alloy as the molding material has been developed [**12, 1, 4, 5**]. The strength, light weight, electromagnetic properties, high quality, and appearance of magnesium alloys have made them particularly attractive for use in electronics products, such as cell phones, digital cameras, and casing for laptop computers, and for use in the automotive industry. It has also been used in many other products ranging from snowboard bindings to tray bases for gas chromatographs.

An injection molded product is made by first feeding the starting material into a hopper that leads into the barrel of the injection molding machine. When the material enters the barrel, it is heated to the appropriate melting temperature by heating bands that encircle the barrel. Inside the barrel, there is a hydraulic piston, consisting of a flange (the tail end), a piston rod, and a screw that is attached to the end of the piston rod. The screw is turned to auger the melted material forward until an amount of material that is sufficient to fill the mold is in front of the tip of the screw. At this point, the screw stops turning, and a variable hydraulic force, that is applied to the piston flange, accelerates the piston and begins to force the melted material into the mold. The applied force is then adjusted in order to keep the piston moving at a constant velocity, where a maximum force can be applied. In normal operation, the piston screw, travelling at the prescribed velocity, will force the molten material to completely fill the mold, at which point it will effectively impact the material in the mold, ensuring that the molten material has completely filled the mold. Once the mold is filled, it is cooled to a temperature that allows the material to solidify, at which time the plates of the mold can be pulled apart, and the product can be ejected from the mold. This process may involve more steps, depending on the material of interest (see, e.g., [**3**]).

Most of the recent research on injection molding has focused on product quality and economic issues associated with the product. In particular, the effects on the final product due to variations in temperature, injection speed, pressure and shear imparted on the material as the screw augers the material forward, and as the piston forces the material into the mold, are investigated in, for example, [**15, 9, 7**], and the effects of the cooling phase on shrinkage, warpage, and other defects of the products are studied in, for example, [**17, 18**]. In addition, much attention has been paid to the materials used in the process because these have significant effect on production costs and product quality (see in particular, [**4, 5**] for the development of magnesium alloys). There are also many papers that present optimization methods that attempt to determine the process parameters that minimize defects and maximize profits [**20, 14**]. Similarly, software has been developed that addresses issues in mold design and material flow during the mold filling process [**11, 6, 13**].

There are, however, relatively few papers that address the effects of the process parameters on the injection molding machine itself. A company that manufactures injection molding machines introduced this question to us at the 8th PIMS-MITACS Industrial Problem Solving Workshop; see [**16**]. Of particular interest to the company were these issues in the context of magnesium alloy being the molding material.

It is desired that the injection molding machine be designed for (essentially) infinite life. Therefore, design features must be specified so that the machine can withstand the repeated strain on the piston due to the impact of the piston screw on the molten metal. In addition, in the event that there is an insufficient amount of material in the mold, the piston may "bottom out." That is, the flange of the piston may impact the housing at full velocity. The machine must also be designed to withstand such impacts.

Factors that affect productivity, such as cycle time and material, must also be considered in the design of the machine. For example, cycle times may be increased by increasing piston velocity. However, any damage to the machine resulting from such an increase will greatly outweigh any benefit of a shorter cycle time. Therefore, in order to efficiently engineer the machine, it is necessary to understand how various features of the process and the machine's design affect the forces of impact. The company was using a transient finite-element analysis (FEA) to study these effects. However, an FEA is not only time consuming but the company's FEA resources are limited. Therefore, a simplified model, that could be used by a designer to obtain a first pass type of analy-

sis, is desired. Once appropriate design features are obtained using the simplified model, they can be verified using an FEA.

We derive a series of simplified models that can be used to generate pressure profiles that occur during impact. The profiles can be used to determine if the impact is likely to cause damage to the machine. Of particular interest are the forces involved in the impact of the screw on the molten metal, and the impact of the piston flange on the injection housing (i.e., when the piston "bottoms out"). In the models, we include a variety of features that may affect the impact forces, and determine whether their contributions are significant. For the impact of the screw, we consider the molten metal's bulk modulus (alternatively, its compressibility), and the leakage of the molten metal past the impacting screw tip created by clearances between the screw and the housing (see Figure 1). The company's analysis of the "bottom out" problem originally assumed a dry contact between the piston flange and injection housing, when, in fact, there is a thin film of hydraulic fluid between the impacting bodies that is expected to reduce the strain on the system. We also consider this effect.

Because magnesium alloys generally have compressibilities much lower than those of plastics and because bottoming out generally occurs more frequently in the injection molding of magnesium alloys, the issues that we address in this paper tend to be of greater concern in the injection molding of a magnesium alloy. However, much of what we discuss can be applied with little modification to the injection molding of other materials.

We begin our investigation of the importance of the presence of the hydraulic fluid, the compressibility of the molten metal, and the leakage past the screw tip, by deriving a simple model (Section 2) in which we assume that the deformation of the piston and housing may be ignored. From this model we can estimate the pressure in the film of hydraulic fluid, and the pressure in the mold. In Section 3, we distinguish parameter regions in which the major forces that bring the piston to rest are in the film or in the mold. In cases where the film force dominates, the magnitude of the pressure is found to be sufficiently large that elastic deformations of the piston and housing will be of the same order of magnitude as the changes in the film thickness. Therefore, in Section 4, we consider a mass-spring model that assumes elastic deformation of the machine parts. The model is derived so that it agrees with a continuous one-dimensional model in two specific test cases. The mass-spring model is verified by comparison with the solutions from a continuous model that assumes that deformations of the machine parts are governed by

the one-dimensional elastic wave equation. Further consideration of the film pressure reveals that it is also sufficiently large to bring about pressure related changes in the viscosity. This is discussed in Section 5. The variable viscosity is relatively easily handled in the mass-spring model. However, it leads to substantial difficulties in the solution method for the continuous elastic model. We also propose a model that combines results from the mass-spring model with those of the continuous model. This hybrid model can easily accommodate the variable viscosity, but also maintains some of the detail of the continuous model. Comparisons between different models are given.

2 A simple model There are two phases in each piston action: (1) constant velocity, and (2) constant applied force. The first occurs at the beginning of the action, while the piston is moving relatively freely and the applied force is sufficient to maintain the piston moving at constant velocity (i.e., when the piston has not yet forced all the material into the mold, or when the piston flange has not come close to the housing). In the second phase, even the maximum applied force is insufficient to maintain the piston at constant velocity, and the piston begins to decelerate. Because maximum pressure occurs in the second phase, we will focus on this phase, during which the maximum applied force is applied throughout.

We begin by writing down equations of motion for the piston, i.e., the familiar $F = Ma$ equations, where M is the mass of the piston, $a = d^2h/dt^2$ is the acceleration of the piston, h is the position of the piston, and F is the sum of the forces on the piston. We choose $h = 0$ as the position for which the piston flange is in contact with the housing, and such that it is always positive, i.e., h represents the width of the gap between the flange and the housing; see Figure 1. The acting forces include the applied force F_{app}, which in the second phase of motion is constant, the force F_m due to impact with the molten metal in the mold, and the force F_f due to the impact of the piston flange and the housing. Due to the presence of hydraulic fluid between the piston flange and the housing, this force is felt before the piston flange contacts the machine housing because the flange is required to displace the hydraulic fluid as it approaches the housing. The equation of motion for the piston is:

$$M\frac{d^2h}{dt^2} = F_f + F_m - F_{\text{app}}, \tag{1}$$

where F_{app} is held constant at the maximum applied force i.e. $F_{\text{app}} = F_{\max} = \text{constant}$. We assume that the constant $F_{\text{app}} > 0$, and therefore,

because it acts to decrease the gap h, we must subtract it in the sum of forces in (1). In the next two subsections we derive forms for the forces F_f and F_m.

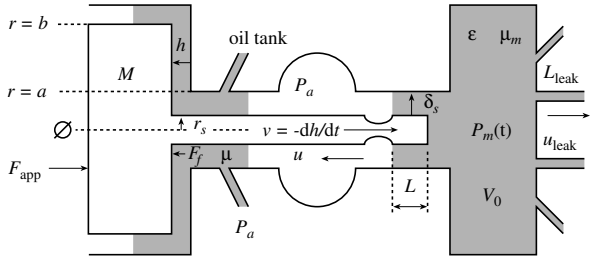

FIGURE 1: Schematic diagram of the injection molding machine.

2.1 Modelling the squeeze film between the flange and housing
It is well-known that lubricants can support high loads in sufficiently small gaps. A lubricant will act to prevent contact between moving components and reduce stress by spreading the load. This is the reason that automobile or machine parts exhibit very little wear when adequately lubricated. The process may be modelled by the lubrication approximation to the Navier-Stokes equations.

When a two-dimensional flat indenter is pressed onto an elastic surface, a stress singularity occurs at the edges of the indenter (in practise, some plastic deformation will occur to reduce this). For this reason it is common practise to round edges and so prevent excessively high stresses. When a fluid is placed between the indenter and the elastic body the fluid forms what is known as a squeeze film. The pressure in the squeeze film is highest at the centre and reduces to the ambient pressure at the edges of contact. Obviously the stress distribution is completely different from the case when there is no fluid present, with the lubricated contact being much less likely to exhibit stress related wear. Hence modelling a lubricated contact with a dry contact model will always lead to drastically different behaviour to the true situation.

Due to the presence of hydraulic fluid between the piston flange and the housing, a squeeze film analysis is appropriate for this region. We consider the normal motion of the piston flange toward the stationary, rigid machine housing, while the hydraulic fluid flows out of the region

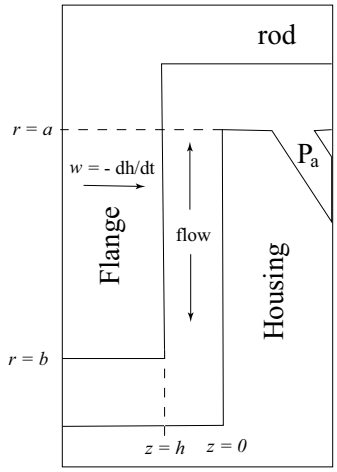

FIGURE 2: Detail of the region between the flange and housing.

of contact; see Figure 2. We model the flow of the hydraulic fluid by the Navier-Stokes equations in the standard lubrication limit, where we assume that gravity is negligible, that the flow is axisymmetric, that the fluid is Newtonian, isoviscous and incompressible, and that the surfaces of the impacting bodies are parallel. Written in cylindrical coordinates (r, z, ϕ), the equations for the fluid velocity u in the radial direction, the fluid velocity w in the z direction, and the pressure p become

$$-\frac{\partial p}{\partial r} + \frac{\partial}{\partial z}\left(\mu_0 \frac{\partial u}{\partial z}\right) = 0, \tag{2}$$

$$\frac{\partial p}{\partial z} = 0, \tag{3}$$

$$\frac{1}{r}\frac{\partial}{\partial r}(ru) + \frac{\partial w}{\partial z} = 0, \tag{4}$$

where $r \in [a, b]$ is the radial coordinate, a and b are the inner and outer radii of the flange, $z \in [0, h]$ is the coordinate along the axis of symmetry of the machine and $z = 0$ at the housing, h is the height of the squeeze film, i.e., it measures the gap between the flange and housing, ϕ is the azimuthal coordinate, and μ_0 is the viscosity of the hydraulic fluid, which is assumed to be constant. The fluid velocity in the azimuthal direction is zero. Equation (2) shows that the dominant force driving the flow

in the radial direction is the pressure gradient, this balances with the viscous resistance that acts to slow down the flow. Equation (3) shows us that the pressure only varies in the radial direction. Equation (4) is the continuity equation for an incompressible fluid.

This system of equations requires solving subject to no-slip conditions at the solid surfaces, i.e., $u = 0$ at $z = 0, h$, $w = 0$ at $z = 0$ and $w = -\partial h/\partial t$ at $z = h$. The pressure is ambient, $p = P_a$ at $r = a$, due to the presence of the outlet; at $r = b$ the fluid exits into a larger, constant pressure region, thus $\partial p/\partial r = 0$ here.

Equation (3) indicates $p = p(r, t)$, and thus, (2) can be integrated twice with respect to z to obtain

$$u = \frac{1}{2\mu_0}\frac{\partial p}{\partial r} z(z - h), \tag{5}$$

where the no-slip boundary conditions for u have been applied. Integration of the continuity equation (4) across the film (i.e., with respect to z) leads to

$$w(h) - w(0) = -\frac{\partial h}{\partial t} = -\frac{1}{r}\frac{\partial}{\partial r} r \int_0^h u \, dz. \tag{6}$$

Note, the derivative may be taken outside the integral because $u = 0$ on the upper and lower surfaces. We now substitute u given in (5) into (6), and evaluate the integral to obtain

$$\frac{\partial h}{\partial t} = \frac{1}{r}\frac{\partial}{\partial r}\left(\frac{r h^3}{12\mu_0}\frac{\partial p}{\partial r}\right). \tag{7}$$

In the case of a rigid, flat flange, the surface has a height that decreases with time only, i.e. $h = h(t)$. In particular, the height h is not a function of r, and thus, (7) may be integrated twice. After applying the pressure boundary conditions, we obtain the equation describing the pressure p in the squeeze film

$$p = P_a + 6\mu_0 \frac{1}{h^3}\frac{dh}{dt}\left[\frac{r^2 - a^2}{2} - b^2 \log\frac{r}{a}\right], \tag{8}$$

where $\partial h/\partial t = dh/dt$ because h is only a function of time t. Finally, the force F_f on the piston due to the film is

$$F_f = 2\pi \int_a^b rp \, dr = \pi P_a (b^2 - a^2) - 6\mu_0 I \frac{1}{h^3}\frac{dh}{dt}, \tag{9}$$

where

$$I = \frac{\pi}{4}\left[4b^4 \log\frac{b}{a} - (3b^2 - a^2)(b^2 - a^2)\right]. \tag{10}$$

2.2 The piston screw—molten metal impact We now derive the form of the force F_m due to impact of the piston on the molten metal in the mold. If we assume that the pressure in the mold P_m does not depend on the spatial coordinates, then F_m is given by

$$F_m = \pi r_s^2 P_m, \tag{11}$$

where r_s is the radius of the screw tip (which we assume is the same as the radius of the piston rod), i.e., πr_s^2 is the cross-sectional area of the screw tip. Thus, to close the system, we must find an equation that gives the time dependence of P_m. Because it is expected that both the compressibility of the molten metal and the leakage of the molten metal past the screw tip will decrease the strain on the system, we will include both.

We begin with the equation for the conservation of mass of the molten metal. That is, we obtain an equation indicating that the rate of change of mass within the mold is equal to the rate at which the mass leaves the mold. The mass is written as density ρ_m times volume V of the mold, where $V = V(t)$ is defined as the volume on the mold side of the screw tip. It is assumed that the density can be written as a function of the pressure P_m in the mold only, and that the pressure $P_m = P_m(t)$ does not depend on the spatial coordinates. In particular, we ignore the effects due to temperature variations of the molten material within the mold. In addition, we neglect the effects due to the flow through the entrance of the mold induced by the compression of the molten metal, and any other effects due to the geometry of the screw tip and mold. The leakage flow out of the mold, denoted as u_{leak} in Figure 1, can be ignored because, when material enters these channels (i.e., which we assume occurs only after the mold is full), it solidifies very quickly due to increased cooling and blocks any further flow.

As is the case for the squeeze film, the process occurs in two stages, the first is a constant velocity stage, while the second is a constant load phase. We assume that the stage of interest is the second, and that at the beginning of this stage the mold has been filled (no holes) and the initial velocity of the piston is the velocity that is prescribed during the first stage.

The conservation of mass gives the equation

$$R_m + R_l = 0, \tag{12}$$

i.e., the rate of change of mass within the mold, R_m, is equal to the rate at which the mass leaves the mold R_l. The rate of change R_m of the mass within the mold is given by

$$R_m = \frac{d}{dt}\left[\rho_m(P_m)V(t)\right] \tag{13}$$

$$= V(t)\frac{d}{dt}\left[\rho_m(P_m)\right] + \rho_m(P_m)\frac{dV(t)}{dt}. \tag{14}$$

The volume $V(t) = V_0 + \pi\left(r_s + \delta_s\right)^2 h$, where V_0 is the volume in the mold when $h = 0$, h gives the position of the piston, r_s is the radius of the screw tip (and the piston rod), and δ_s is the gap width between the screw tip and the housing. If we choose V_0 to be the volume $V(t)$ when the piston flange is in contact with the housing, then the h representing the position of the piston will correspond to the height h of the squeeze film defined in Section 2.1; this is the motivation for choosing this notation. We will assume that $\delta_s \ll r_s$, and thus will be neglected in the equation for the mold volume, which becomes

$$V(t) = V_0 + \pi r_s^2 h. \tag{15}$$

With (15) and the assumption that the pressure P_m in the mold is only a function of time t, (14) becomes

$$R_m = \epsilon\rho_m(P_m)V(t)\frac{dP_m}{dt} + \pi r_s^2\rho_m(P_m)\frac{dh}{dt}, \tag{16}$$

where

$$\epsilon = \frac{1}{\rho_m}\frac{\partial\rho_m}{\partial P_m} \tag{17}$$

is the compressibility of the molten metal.

Now we look at the rate R_l at which the mass passes the screw tip (and flows through the gap between the piston rod and the housing). With the assumption that $\delta_s \ll r_s$, the effects of the curvature of the piston and housing become negligible, and we obtain

$$R_l = 2\pi r_s\delta_s\overline{u}\rho_m(P_m), \tag{18}$$

where $\overline{u}$ is the average velocity of the fluid passing the screw tip.

To find $\overline{u}$, we can assume that we have Couette flow in the gap between the screw tip and the housing, because the flow is expected to be laminar [**4**]. In this case, with the assumption of negligible curvature, the fluid velocity is axisymmetric (i.e., it does not vary in the azimuthal direction), and it does not vary lengthwise along the gap, and thus, $\overline{u}$ is given as the average of u, the velocity of the fluid in the lengthwise direction along the gap. A magnification of the region of interest is drawn in Figure 3. The velocity $u = u(y)$ of the fluid in the gap is given by

$$\frac{d^2u}{dy^2} = -\frac{P_m - P_a}{\mu_m L}\,, \tag{19}$$

where $y \in [0, \delta_s]$ gives the position across the gap from the housing ($y = 0$) to the screw tip ($y = \delta_s$), i.e., $y = r_s + \delta_s - r$, $P_m = P_m(t)$ is the pressure in the mold, P_a is the pressure inside the housing, which will be assumed to be the same as the ambient pressure discussed in section /refsec:filmder, μ_m is the (constant) viscosity coefficient of the molten metal, and L is the length of the screw tip. We will assume that L is constant, which implies that if the gap is not already filled with the molten metal, then the filling has negligible effect. This assumption is reasonable because we have $\delta_s \ll r_s$ and $L \sim O(r_s)$, which implies that the piston need only move $O(\delta_s)$ in order to fill the gap; we expect that the distance the piston moves is much greater than this.

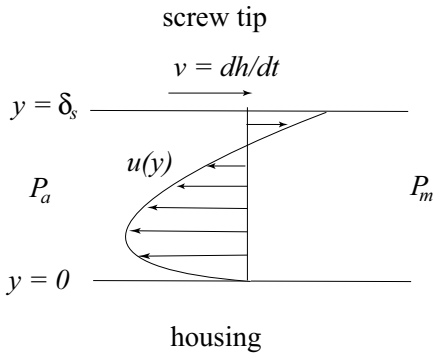

FIGURE 3: Couette flow in the gap between the screw tip and the housing.

With no-slip conditions at the boundaries, i.e., $u = 0$ at $y = 0$, and $u = dh/dt$ at $y = \delta_s$, where h and dh/dt give the position and velocity of the piston, respectively, we find that the fluid velocity $u(y)$ is given by

$$u = \frac{P_m - P_a}{2\mu_m L}\left(\delta_s y - y^2\right) + \frac{1}{\delta_s}\frac{dh}{dt}\,y, \tag{20}$$

and the average velocity

$$\overline{u} = \int_0^{\delta_s} u\,dy = \frac{P_m - P_a}{12\mu_m L}\,\delta_s^2 + \frac{1}{2}\frac{dh}{dt}. \tag{21}$$

We substitute this into (18) and obtain an equation for the rate of mass passing the screw tip:

$$R_l = \pi r_s \rho_m \left[\frac{P_m - P_a}{6\mu_m L}\,\delta_s^3 + \delta_s \frac{dh}{dt}\right]. \tag{22}$$

We substitute (16) and (22) into the equation describing the conservation of mass (12) and rearrange to obtain the desired equation describing the rate of change dP_m/dt of the pressure in the mold P_m in terms of P_m, h, dh/dt

$$\frac{dP_m}{dt} = \frac{-\pi r_s}{\epsilon\left(V_0 + \pi r_s^2 h\right)}\left[(r_s + \delta_s)\frac{dh}{dt} + \frac{P_m - P_a}{6\mu_m L}\delta_s^3\right]. \tag{23}$$

Assuming that $\delta_s \ll r_s$, this reduces to

$$\frac{dP_m}{dt} = \frac{-\pi r_s}{\epsilon\left(V_0 + \pi r_s^2 h\right)}\left[r_s\frac{dh}{dt} + \frac{P_m - P_a}{6\mu_m L}\delta_s^3\right]. \tag{24}$$

2.3 The simple model and its behaviour When the expressions for the force F_f in the squeeze film and the force F_m in the mold, given by (9) and (11), respectively, are substituted into (1), the equations describing the motion of the piston, along with the equation (24) for the rate of change dP_m/dt of the pressure in the mold, become a coupled system of differential equations with dependent variables h (representing both the height of the squeeze film and the position of the piston) and P_m (the pressure in the mold). The resulting are

$$M\frac{d^2h}{dt^2} = -6\mu_0 I\frac{1}{h^3}\frac{dh}{dt} + \pi r_s^2 P_m + \pi\left(b^2 - a^2\right)P_a - F_{\text{app}}, \tag{25}$$

$$\frac{dP_m}{dt} = \frac{-\pi r_s}{\epsilon\left(V_0 + \pi r_s^2 h\right)}\left[r_s\frac{dh}{dt} + \frac{P_m - P_a}{6\mu_m L}\delta_s^3\right], \tag{26}$$

where $V(t) = V_0 + \pi r_s^2 h$ is the volume of the molten metal inside the mold, ϵ is the compressibility of the molten metal, μ_0 is the viscosity of the hydraulic fluid, μ_m is the viscosity of the molten metal, M is the mass of the piston (including the piston flange, piston rod and the screw), F_{app} is the (constant) force applied to the piston during the second stage (i.e., $F_{\text{app}} = F_{\max}$), P_a is the ambient pressure, r_s is the radius of the screw tip (assumed equal to the radius of the piston rod), δ_s is the width of the gap between the screw and the injection housing, L is the length of the screw tip, and

$$I = \frac{\pi}{4}\left[4b^4 \ln\frac{b}{a} - \left(3b^2 - a^2\right)\left(b^2 - a^2\right)\right], \tag{27}$$

i.e., a constant that depends on b and a, the radius of the flange (or the flange width) and the radius of the housing along the length of the piston rod, respectively. Equation (25) describes the deceleration of the piston, which depends on the unknown functions describing the height h of the squeeze film (as well as its rate of change dh/dt) and the pressure P_m in the mold, and which also depends on the parameters, the ambient pressure P_a and the maximum applied force F_{app}. Equation (26) describes the pressure within the mold. This depends on the rod motion (which depends on the squeeze film thickness) and the leakage between the screw tip and housing.

We non-dimensionalise using the following scaling factors:

$$h = h_0 x_1, \qquad \frac{dh}{dt} = \frac{h_0}{t_0} x_2, \qquad P_m - P_a = P_0 x_3, \tag{28}$$

and rescale t by t_0, i.e., x_1 is the scaled height of the squeeze film, x_2 is the scaled piston velocity, and x_3 is the scaled pressure in the mold. The equations of motion become

$$\dot{x}_1 = x_2, \tag{29}$$

$$\dot{x}_2 = -\alpha\frac{x_2}{x_1^3} + \beta x_3 - f_{\text{app}} + \beta\left(\frac{r_s^2 + b^2 - a^2}{r_s^2}\right)\frac{P_a}{P_0}, \tag{30}$$

$$\dot{x}_3 = \frac{1}{1 + \delta x_1}\left[-x_2 - \gamma x_3\right], \tag{31}$$

where the dot represents a derivative with respect to non-dimensional time, t_0 is defined as h_0/v_{init}, v_{init} is the initial velocity of the piston

(i.e., the velocity prescribed in the first stage of the impact). In addition,

$$P_0 = \frac{Mv_{\text{init}}^2}{h_0 \pi r_s^2} = \frac{1}{\varepsilon} \frac{\pi r_s^2 h_0}{V_0}, \tag{32}$$

where the first equality describes the pressure required to stop the moving piston in a distance h_0, while the second equality describes the pressure induced by compressing the molten metal a distance h_0 (equating these can produce an expression for h_0). The system is controlled by six dimensionless parameters, the aspect ratio δ_s/r_s, (i.e., the ratio of the gap width to the radius of the piston rod), and five others α, β, γ, δ, and f_{app}, which are related to the physical parameters as follows:

$$\alpha = \frac{6I\mu v_{\text{init}}/h_0^2}{Mv_{\text{init}}^2}, \tag{33}$$

i.e., α is the ratio of the energy dissipated in the squeeze film to the initial energy,

$$\beta = \frac{P_0 h_0 \pi r_{rod}^2}{Mv_{\text{init}}^2} = \frac{\frac{\Delta V}{\varepsilon}\frac{\Delta V}{V_0}}{Mv_{\text{init}}^2}, \tag{34}$$

(where $\Delta V = \pi r_s^2 h_0$ is the change in the volume V of molten metal in the mold corresponding to a change in piston position h of h_0), i.e., β is the ratio of the energy required to compress the molten metal a distance h_0 to the initial energy, which by definition implies that $\beta = 1$,

$$\gamma = \frac{P_0 t_0 \delta_s^3}{6 r_s h_0 L_0 \mu_m} = \frac{2\pi \delta_s r_s \frac{P_0 \delta_s^2}{12 \mu_m L_0}}{\pi r_s^2 v_{\text{init}}}, \tag{35}$$

i.e., γ is the ratio of the leakage flow rate at maximum compression to the initial flow rate,

$$\delta = \frac{h_0 \pi r_s^2}{V_0} \ll 1, \tag{36}$$

i.e., δ is the ratio of volume of compression of molten metal to volume of the mold, and

$$f_{\text{app}} = \frac{t_0^2 F_{\text{app}}}{h_0 M} = \frac{h_0 F_{\text{app}}}{Mv_{\text{init}}^2} \tag{37}$$

is the non-dimensionalised applied (constant) force, i.e., f_{app} is the ratio of work done by the applied force over a distance h_0 to the initial energy.

Because δ is very small, it may be neglected and therefore, there are only five parameters that control the motion of the piston. In addition, we expect that $P_a/P_0 \ll 1$, and thus, the last term in (30) can also be neglected.

We now carry out some numerical calculations to demonstrate the various possible types of behaviour that can be observed. For example, we expect that if there is little leakage of molten metal past the screw tip, then the piston will be stopped by the molten metal. However, if there is significant leakage, then it will be the squeeze film that acts to stop the motion. In the first example, we choose the gap width between the screw and the injection housing $\delta_s = 70\mu$m, which is a reasonably large gap through which the molten metal may pass. The results of the numerical calculations, shown in Figure 4(a),(b), indicate that most of the load of the impact is taken by the squeeze film, with only a very small load taken by the mold. The squeeze film height h initially decreases rapidly and then slowly tends to a constant (non-zero) value. The velocity of the piston has a corresponding initial stage when it changes slowly, and then a stage, corresponding to a peak in the squeeze film force, when it rapidly tends to zero. The scaled pressure starts at a low value and then increases rapidly as impact is approached. As the piston velocity decreases, the pressure decreases until it reaches a low value sufficient to balance the applied force. In this case, the dimensional squeeze film force F_f reaches a maximum of just over 8×10^6 Newtons, while the maximum of the dimensional mold force F_m is approximately 100 times smaller.

As the gap width δ_s decreases, there is less leakage and more of the load is taken by impact of the screw on the molten metal. Calculations for the case when the gap width δ_s is 35μm are shown in Figure 4(c),(d). As in the previous case, the squeeze film height h initially decreases rapidly. However, the relaxation of the film height h to the constant value is slower, and the deceleration of the piston is not as sharp. Of particular interest is that an increase in the dimensional force F_m in the mold is observed, although it is still about 10 times smaller than the squeeze film force.

If the gap width δ_s is taken to be as small as 10μm (very little leakage), there seems to be a qualitative change in the solution. In this case, the initial kinetic energy of the piston goes almost fully into compressing the molten metal, i.e. the squeeze film takes little of the burden. This compression is assumed to be elastic, and thus, because there is very

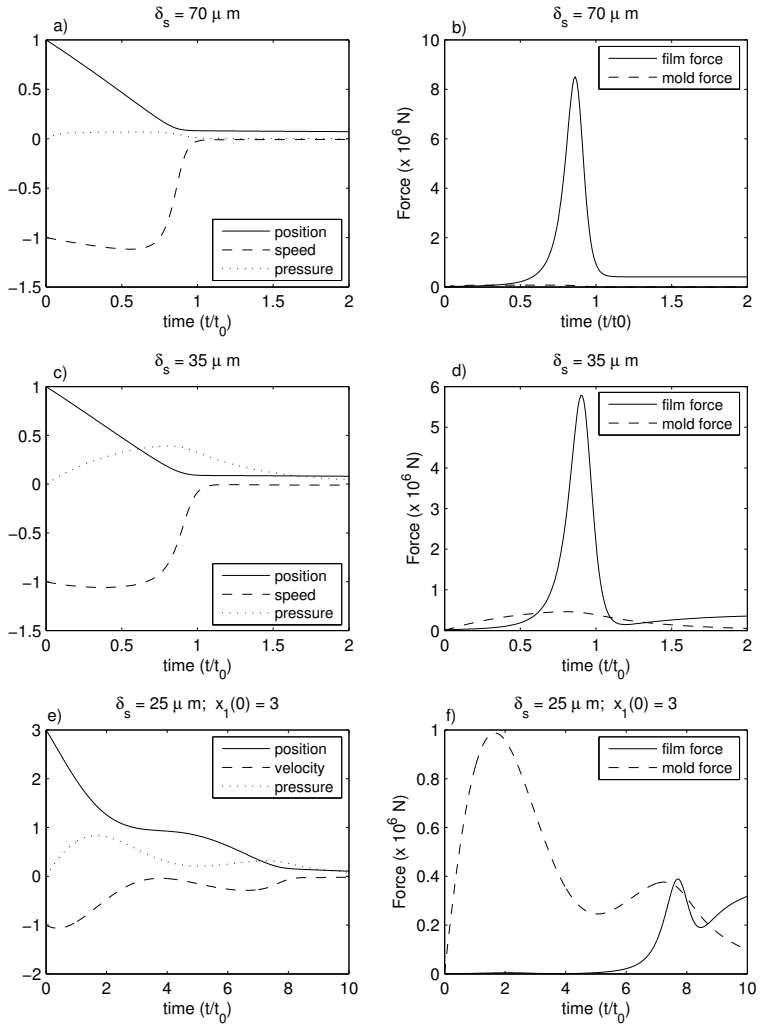

FIGURE 4: Results of simulation: (a) and (b) high leakage with the gap width $\delta_s = 70\mu$m; (c) and (d) moderate leakage with the gap width $\delta_s = 35\mu$m; (e) and (f) low leakage and large run up with the gap width $\delta_s = 25$ and initial position = 2.5. Position, speed and pressure, plotted in a), b), and c), refer to the non-dimensionalised variables, x_1, x_2 and x_3, respectively. These are related to the dimensional quantities via (28). Dimensional forces are plotted in b), d), and f), with time scaled by t_0.

a	0.05 m
b	0.1 m
δ_s	5×10^{-5} m
r_s	3.5×10^{-2} m
M	105 kg
L	1×10^{-2} m
V_0	1×10^{-3} m^3
μ_0	1×10^{-2} Ns/m^2
μ_m	1×10^{-3} Ns/m^2
ϵ	1×10^{-11} m^2/N
F_{app}	4×10^5 N
P_a	1×10^5N/m^2
v_{init}	3 m/s

TABLE 1: Table of parameter values that are used for calculations.

little leakage, the piston rebounds, and oscillates. However, because the squeeze film pressure becomes negative when the piston rebounds, our model is not expected to produce valid results when this occurs. This qualitative mold-dominant behaviour can also be seen if the gap width $\delta_s = 25\mu$m, and the initial value of the position $x_1(0) = 3$. The increase in the initial value allows a longer distance over which the mold force can do work. Because the pressure variable x_3 only depends on the rate of change of position x_2, the increase in the initial value has little effect on x_3 (where x_3 corresponds to the dimensional mold pressure), while for the squeeze film, a larger position x_1 implies a smaller squeeze film force. This case is shown in Figure 4(e),(f). In this case, the mold force takes the initial load, while the film force only becomes evident when the position variable becomes very small. The oscillatory behaviour of the variable is due to the elastic property of the material in the mold. The velocity does not become negative, and thus the film pressure is always positive.

The definition (33) of the dimensionless parameter α indicates that as α increases, the effects of the squeeze film become more important. In particular, in the case when both the dimensionless parameter α and the gap width δ_s are large, the full impact of the piston is absorbed by the squeeze film, i.e., this corresponds to the situation when there is no molten metal in the mold. The parameter α can be increased by increasing the value of I (see equation (27)) which in turn can be

increased by increasing the flange width b. The results of increasing the dimensionless parameter α (not shown) are qualitatively similar to the situation shown in Figure 4(a),(b), except that there is a sharper deceleration of the piston on impact, and a corresponding increase in the squeeze film force. In Section 3, we extend our discussion of the various limits of the simple model.

In order to more easily see the form of the force profiles, we plot in Figure 5 the force F_f in the squeeze film and the force F_m in the mold as a function of time for the case when the gap width $\delta_s = 50\mu$m The maximum of the squeeze force F_f in dimensional units is over 7×10^6Newtons, while the maximum force in the mold is over 30 times smaller. This pressure in the squeeze film is felt over only a small area near the outside of the flange; the pressure decreases rapidly toward the inner part of the flange. To illustrate this, the pressure in the squeeze film, as given by (8), as both a function of time and distance along the flange, is plotted in Figure 6.

3 Limits of the simple model To gain insight into the behaviour of our simple model, we explore the model's various operational limits. We consider the following system:

$$\dot{x}_1 = x_2, \tag{38}$$

$$\dot{x}_2 = -\alpha \frac{x_2}{x_1^3} + x_3 - f_{\text{app}}, \tag{39}$$

$$\dot{x}_3 = -x_2 - \gamma x_3, \tag{40}$$

which are (29)–(31) with P_a/P_0, δ assumed to be negligible, as discussed above. Initial conditions are:

$$x_1(0) = x_0, \qquad x_2(0) = -1, \qquad x_3(0) = 0, \tag{41}$$

i.e., x_0 represents the initial gap, we have scaled with the initial velocity, hence $x_2(0) = -1$, and the mold pressure is initially assumed to be approximately P_a, the pressure in the screw chamber.

We see that the leading order behaviour of our system is governed by α, f_{app}, γ and x_0. We have seen that there are essentially two limiting domains of operation: one in which the effects due to the squeeze film are dominant, and another in which the effects of the impact of the piston on the mold are dominant. In this section, we delineate these operating regimes in terms of α, f_{app}, γ and x_0.

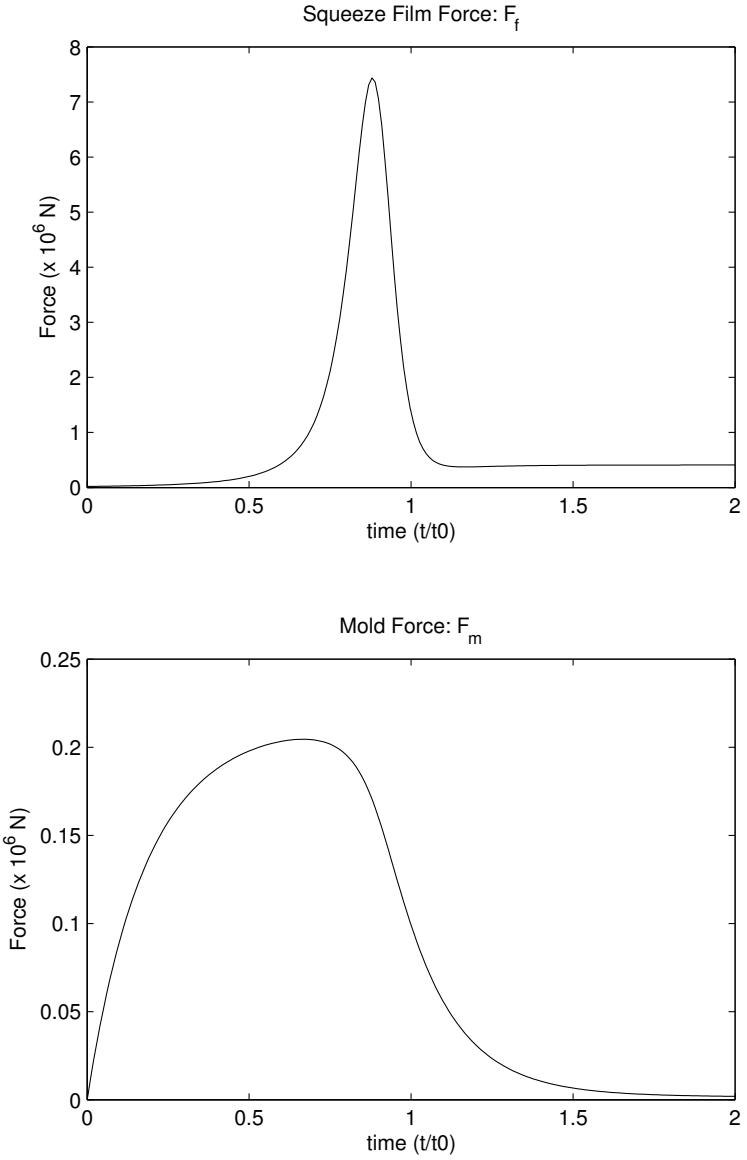

FIGURE 5: Dimensional force F_m in mold and dimensional force F_f in squeeze film, with $\delta_s = 50\mu$m.

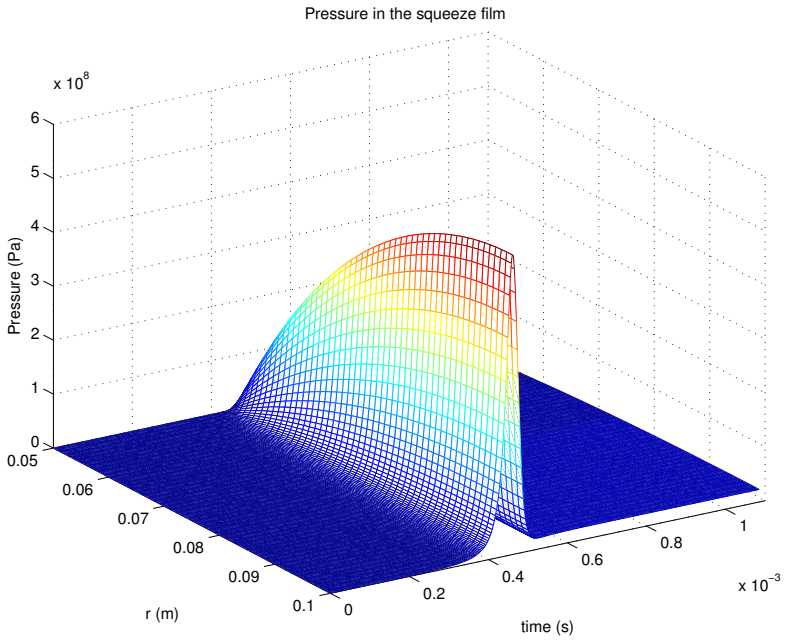

FIGURE 6: Dimensional pressure in squeeze film vs. dimensional time t and radial coordinate r, with $\delta_s = 50\mu$m.

3.1 Dominant mold regime We observe from (39)–(40) that x_3 initially grows to an $O(1)$ value, over a timescale of $O(1)$. We therefore assume *a priori* that $x_0 \sim O(1)$ and that $\alpha x_2/x_1^3 \ll |x_3 - f_{\text{app}}|$ over some initial period. Given the initial conditions on x_2 and x_3, a necessary condition for this is the assumption that initially

$$\alpha/x_0^3 \ll f_{\text{app}}. \tag{42}$$

With these assumptions, the term representing the effects of the squeeze film will be negligible, and our approximate system becomes

$$\dot{x}_1 = x_2, \tag{43}$$

$$\dot{x}_2 = x_3 - f_{\text{app}}, \tag{44}$$

$$\dot{x}_3 = -x_2 - \gamma x_3, \tag{45}$$

which is linear. From (44)–(45), we derive:

$$\ddot{x}_3 + \gamma \dot{x}_3 + x_3 = f_{\text{app}}, \quad x_3(0) = 0,\ \dot{x}_3(0) = 1. \tag{46}$$

Therefore, in the absence of the squeeze film, the system behaves as a damped linear oscillator. If we solve (46) to find the pressure x_3, then we can find the speed x_2 and gap width x_1 by integrating (43) and (44).

Because the particular solution is $x_{3,p} = f_{\text{app}}$, and $\gamma > 0$ implies decay of the homogeneous part, the only differences in qualitative behaviour are due to changes in γ. We look for solutions of (46) of the form $e^{\sigma t}$, and find that for $\gamma > 2$, σ is real, and we are in the overdamped regime. For $\gamma < 2$, there are oscillatory solutions, and we are in the underdamped region.

As discussed in Section 2.3, γ represents the ratio of leakage rate out of the mold to rate of compression. Because leakage occurs only due to build up of pressure in the mold (from compression), on physical grounds we should expect that $\gamma < 1$ (i.e., when $\gamma > 1$, compressibility has little effect in stopping the rod and damping is from the leakage only). Therefore, we expect the underdamped regime to be more applicable here.

3.1.1 *The underdamped regime:* $\gamma < 2$ If we are in the underdamped regime ($\gamma < 2$), then there is an oscillatory timescale: $2\pi/(1-\gamma^2/4)^{1/2}$, and a decay timescale: $2/\gamma$. These are essentially long timescales, and govern the speed at which $x_3 \to f_{\text{app}}$. For reference, in the absence of damping, the timescale for the homogeneous system is 2π.

Examination of (43)–(45) reveals that, when $f_{\text{app}} \gg 1$, the timescale for growth of x_2 is initially $1/f_{\text{app}}$, i.e., $x_2 \sim -1 - f_{\text{app}} t$, and hence

$$x_1 \sim x_0 - t - f_{\text{app}} t^2/2.$$

Therefore, as $t \to (2x_0/f_{\text{app}})^{1/2}$, x_1 becomes small, and the squeeze film term becomes large. In order to remain in the mold dominant regime, we must impose an upper bound on the applied force. Thus, in the underdamped regime, the mold is dominant when f_{app} satisfies:

$$\frac{\alpha}{x_0^3} \ll f_{\text{app}} \ll 2x_0 \max\left\{\frac{1-\gamma^2/4}{4\pi^2}, \frac{\gamma^2}{4}\right\}. \tag{47}$$

With $\gamma < 2$, the solution of (46) can be written as

$$x_3(t) = \mathrm{e}^{-\gamma t/2}\left[\frac{1 - f_{\text{app}}\gamma/2}{\lambda}\sin \lambda t - f_{\text{app}} \cos \lambda t\right] + f_{\text{app}}, \tag{48}$$

where $\lambda = \sqrt{1-\gamma^2/4}$. In Figure 7 the numerical solution of the full non-dimensional system (38)–(40) is compared with the solution. The timescales are clear in this plot. At approximately $t = 2.2$, the pressure begins to drop. Near $t = 3.2$, the approximated pressure begins to deviate from the numerical solution, and at close to $t = 7$, the numerical approximations of all variables approach zero, which implies that the mold regime approximation is not valid any more.

The mold pressure attains its maximum at t_{max}, when

$$\tan \lambda t_{max} = \frac{(f_{\text{app}}\gamma - 1)\sqrt{1-\gamma^2/4}}{f_{\text{app}} - \gamma/2}, \tag{49}$$

where $\lambda = \sqrt{1-\gamma^2/4}$. This is only valid for $f_{\text{app}}\gamma > 1$. Figure 8 shows that the greater the leakage ratio γ, the longer it takes the pressure in the mold to attain the maximum, as was expected.

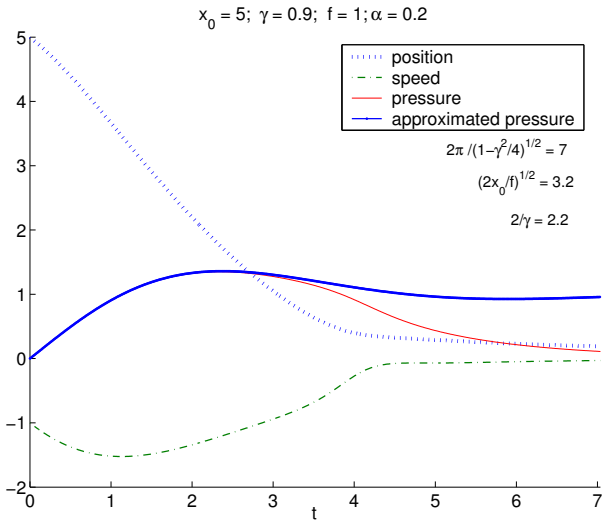

FIGURE 7: Comparison of approximate pressure with numerical computations for an underdamped system, with $x_0 = 5$, $\gamma = 0.9$, $\alpha = 0.2$.

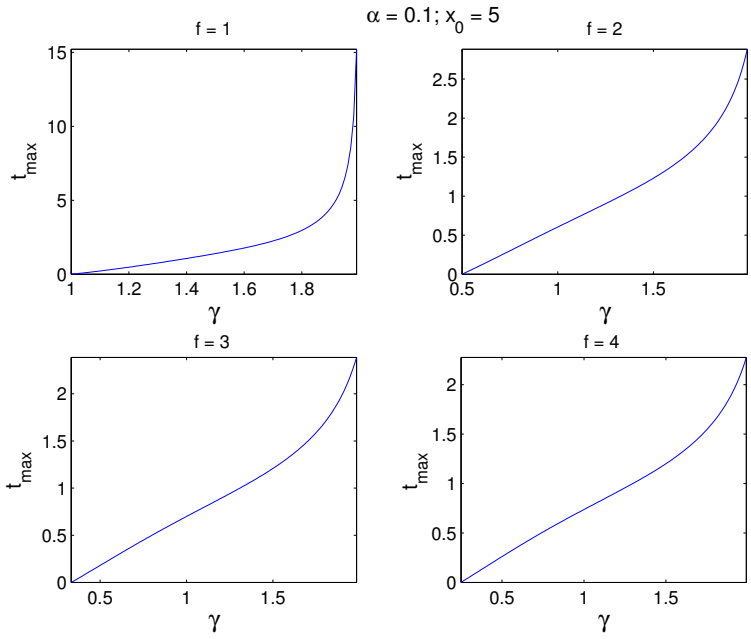

FIGURE 8: Leakage ratio γ vs t_{max} for different forces: the smaller the force, the longer it takes to reach the maximum pressure.

With the pressure x_3 given by (48), and with the initial conditions $x_1(0) = x_0$ and $x_2(0) = -1$, (43) and (44) can be integrated to obtain

$$x_1(t) = \mathrm{e}^{-\gamma t/2}\left[\left(\frac{-2 + 3f_{\mathrm{app}}\gamma + \gamma^2 - f_{\mathrm{app}}\gamma^3}{2\lambda}\right)\sin\lambda t + (f_{\mathrm{app}} + \gamma - f_{\mathrm{app}}\gamma^2)\cos\lambda t\right] - f_{\mathrm{app}}\gamma t + x_0 - (f_{\mathrm{app}} + \gamma - f_{\mathrm{app}}\gamma^2), \tag{50}$$

$$x_2(t) = \mathrm{e}^{-\gamma t/2}\left[\left(\frac{(f_{\mathrm{app}}\gamma - 1)\gamma/2 - f_{\mathrm{app}}}{\lambda}\right)\sin\lambda t + (f_{\mathrm{app}}\gamma - 1)\cos\lambda t\right] - f_{\mathrm{app}}\gamma. \tag{51}$$

Typically, $x_1(t)$ decreases monotonically and eventually the squeeze film terms will become significant. The domain over which the mold dynamics are dominant is therefore defined by the implicit relation:

$$\frac{-\alpha x_2(t_{max})}{x_1^3(t_{max})} \ll |x_3(t_{max}) - f_{\text{app}}|. \tag{52}$$

Figure 9 shows the region in the $f_{\text{app}} - \alpha$ plane where this regime is dominant for fixed values of γ and x_0.

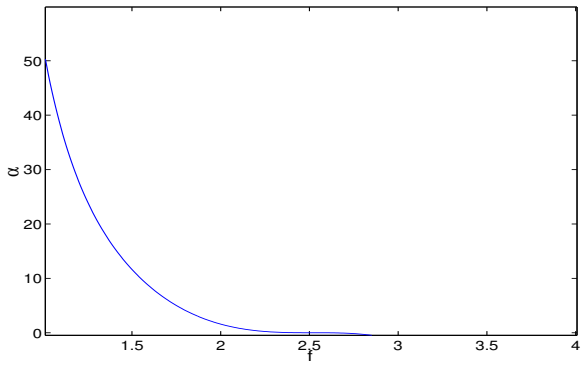

FIGURE 9: Regime in which the mold forces dominant (small α and small f_{app}) in an underdamped system, with $\gamma = 0.9$ and $x_0 = 5$.

3.1.2 *The overdamped regime:* $\gamma > 2$ The overdamped motion is easily analyzed, although, based on the physical argument described above, we believe it is less likely to occur. In this case, the solution to (46) is

$$x_3(t) = \frac{1 + r_2 f_{\text{app}}}{r_1 - r_2} \, \mathrm{e}^{r_1 t} - \frac{1 + r_1 f_{\text{app}}}{r_1 - r_2} \, \mathrm{e}^{r_2 t} + f_{\text{app}}, \tag{53}$$

where

$$r_1 = -\frac{\gamma}{2} + \sqrt{\frac{\gamma^2}{4} - 1}, \qquad r_2 = -\frac{\gamma}{2} - \sqrt{\frac{\gamma^2}{4} - 1}.$$

We substitute this solution for the pressure x_3 into (43)–(44), and integrate to obtain

$$x_1(t) = x_0 + \frac{1 + r_2 f_{\text{app}}}{r_1^2(r_1 - r_2)}[\mathrm{e}^{r_1 t} - 1] - \frac{1 + r_1 f_{\text{app}}}{r_2^2(r_1 - r_2)}[\mathrm{e}^{r_2 t} - 1] - \left[\frac{1 + r_2 f_{\text{app}}}{r_1(r_1 - r_2)} - \frac{1 + r_1 f_{\text{app}}}{r_2(r_1 - r_2)} + 1\right] t, \tag{54}$$

$$x_2(t) = \frac{1 + r_2 f_{\text{app}}}{r_1(r_1 - r_2)}[\mathrm{e}^{r_1 t} - 1] - \frac{1 + r_1 f_{\text{app}}}{r_2(r_1 - r_2)}[\mathrm{e}^{r_2 t} - 1] - 1, \tag{55}$$

Because we have $0 > r_1 > r_2$, we have that $x_3 \to f_{\text{app}}$ exponentially as $\mathrm{e}^{r_1 t} \to 0$ (because the exponential with r_2 decays faster). For large γ and $r_1 t \sim -1$, we have:

$$x_3 - f_{\text{app}} \sim (-f_{\text{app}} + 1/\gamma)\mathrm{e}^{-1}, \tag{56}$$

$$x_1 \sim x_0 - \gamma^2 f_{\text{app}} \mathrm{e}^{-1} - \gamma(1 - \mathrm{e}^{-1}), \tag{57}$$

$$x_2 \sim -1 - (1 - \mathrm{e}^{-1})(f_{\text{app}}\gamma + 1). \tag{58}$$

Thus, to neglect the squeeze film terms in the overdamped regime, as we have seen, we require that

$$\frac{\alpha x_2}{x_1^3} \ll |x_3 - f_{\text{app}}|,$$

which, in this case, leads to

$$\frac{\alpha[1 + (1 - \mathrm{e}^{-1}) f_{\text{app}}\gamma]}{(x_0 - \gamma^2 f_{\text{app}})^3} \ll f_{\text{app}}.$$

Typically this means

$$x_0 \gg \gamma^2 f_{\text{app}}, \tag{59}$$

$$\alpha \ll x_0^3 f_{\text{app}}. \tag{60}$$

The second condition is one we have seen before (see (47)), while the first is new.

Figure 10 shows that the numerical solution of the full nondimensional equations (38)–(40) and the solution given by (56)–(58) are very close for a short period of time.

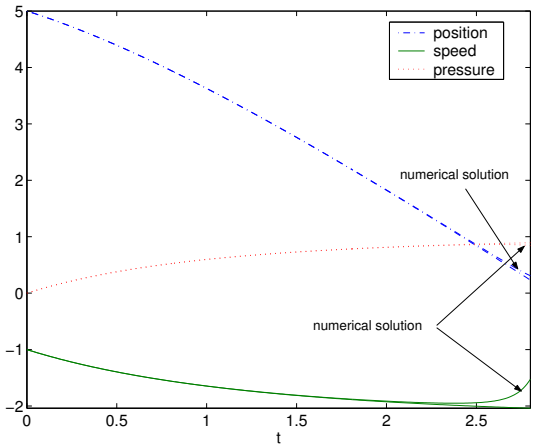

FIGURE 10: Comparison of approximate solutions with numerical computations in the dominant mold and overdamped regime, with $\gamma = 2.2$, $\alpha = 0.1$, $x_0 = 5$ and $f_{\text{app}} = 1$. Approximate and numerical solutions begin to diverge only after $t = 2$.

3.2 Dominant squeeze film regime When $\gamma < 2$, the arguments leading to (47) also indicate that the squeeze film will be dominant if

$$f_{\text{app}} \gg 2x_0 \max\left\{\frac{1-\gamma^2/4}{4\pi^2}, \frac{\gamma^2}{4}\right\}. \tag{61}$$

In this regime, f_{app} is sufficiently large that the compression of the molten metal in the mold does little to slow the progress of the piston; the gap decreases rapidly and eventually the applied force is compensated by the squeeze film. The regions in which we have this large applied force, squeeze film dominant regime are shown in Figure 11.

A second parameter range in which the squeeze film is dominant is where f_{app} is perhaps moderate and the squeeze film term is sufficiently large. Over a short time, since $x_3(0) = 0$, we have:

$$x_2(t) \sim \left[\frac{\alpha}{x_0^3} - f_{\text{app}}\right] t + x_2(0), \quad x_3(t) \sim -\left[\frac{\alpha}{x_0^3} - f_{\text{app}}\right] \frac{t^2}{2},$$
$$x_1(t) \sim x_0 - x_3(t),$$

where we assume that $f_{\text{app}} > \alpha/x_0^3$, so that the pressure remains posi-

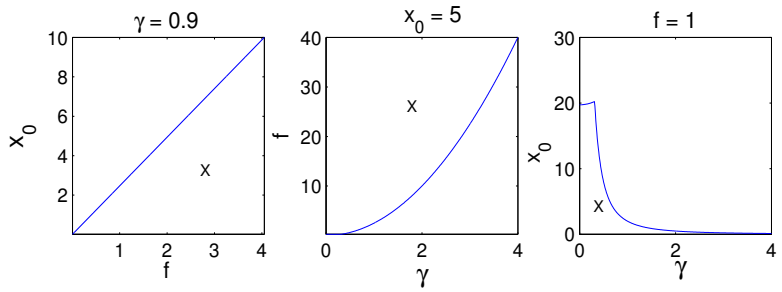

FIGURE 11: Regime in which the squeeze film forces dominant in the case of a large applied force f_{app}. Regions are marked with an X.

tive. The squeeze film term therefore dominates for up until

$$t \sim \frac{2\alpha}{x_0^3}.$$

This is a very short time. For example, for $\alpha = 0.1$ and $x_0 = 2$, this corresponds to $t \sim 0.02$.

However, if on this timescale the film significantly decreases in thickness, the squeeze film term remains dominant. The squeeze film decay time scale (judged from this initial motion) is:

$$t \sim \sqrt{\frac{2}{x_0\left[f_{\text{app}} - \frac{\alpha}{x_0^3}\right]}}.$$

Therefore our second regime for a dominant squeeze film is:

$$\sqrt{\frac{2}{x_0\left[f_{\text{app}} - \frac{\alpha}{x_0^3}\right]}} \ll \frac{2\alpha}{x_0^3}\,. \tag{62}$$

As indicated in Figure 12, a large force, a large α, and a small gap are required to be in this regime.

For either of the above regimes, our reduced system will be:

$$\dot{x}_1 = x_2, \tag{63}$$

$$\dot{x}_2 = -\alpha\frac{x_2}{x_1^3} - f_{\text{app}}, \tag{64}$$

$$\dot{x}_3 = -x_2 - \gamma x_3, \tag{65}$$

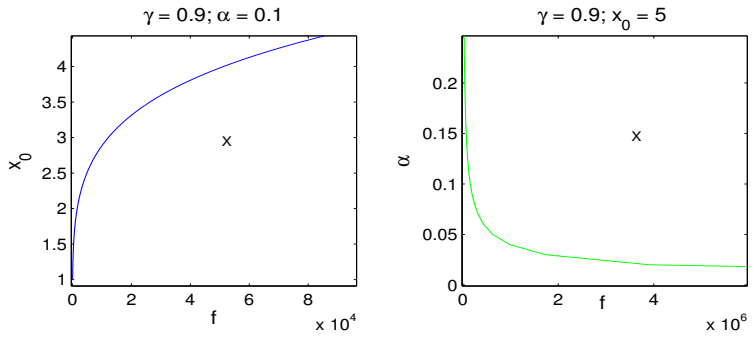

FIGURE 12: Regime in which the squeeze film forces dominant in the case of a small applied force f_{app}. Regions are marked with an X.

i.e., the mold region in (65) decouples. The remaining problem (63) and (64), is a classical squeeze film problem. Integrating once gives:

$$\dot{x}_1 - \frac{\alpha}{2x_1^2} + f_{\text{app}}\, t = -1 - \frac{\alpha}{2x_0^2}, \tag{66}$$

and the solution is known to decay to zero like $t^{-1/2}$. In particular, the film thickness

$$x_1(t) \sim \sqrt{\frac{\alpha}{2 + \alpha/x_0 + 2f_{\text{app}}t}} \sim \sqrt{\frac{\alpha}{2f_{\text{app}}t}}, \quad t \to \infty. \tag{67}$$

Solutions are plotted in Figure 13.

4 Effects of elasticity of piston and housing The basic model described in Section 2 assumes that the elastic deformation of the flange, piston and housing may be ignored. When the Young's modulus of the material is in the range of 100–200 GPa then a force of about 10^7 Newtons will produce displacements that are comparable to our length scale h_0. With forces in the squeeze film reaching values of greater than 8×10^6 Newtons, this effect could become significant. Also, given the pressure loads predicted in the last section, the effects due to the variation of the viscosity of the hydraulic fluid must also be investigated. We defer discussion of this issue to Section 5, while in this section, we extend our simple model to include the elastic deformation of the machine parts.

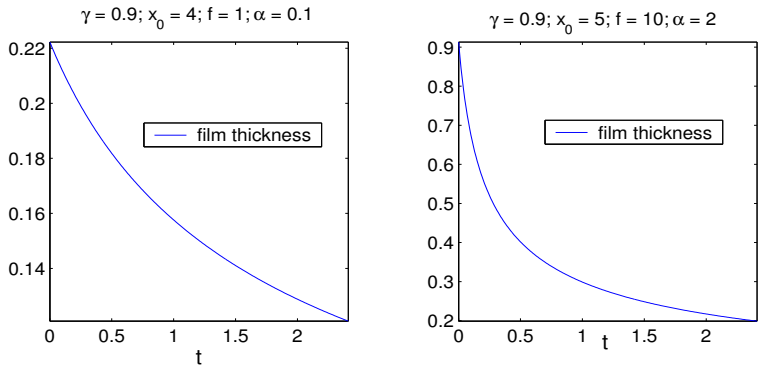

FIGURE 13: Nondimensional film thickness in the squeeze film regime.

We consider three models of varying complexity. First, we consider a discrete model in which the machine parts are modelled with mass-spring systems. Then we consider a simple continuous model in which elastic vibrations are governed by the one-dimensional elastic wave equation. When the variation of viscosity is considered, the solution of the continuous model becomes very difficult. Therefore, we also propose a hybrid model, which retains some of the simplicity of the discrete model while maintaining some of the detail of the continuous model.

4.1 A discrete model with elastic deformation We consider a model in which the machine is separated into three discrete components: the piston flange, the piston rod, and the housing, as shown in Figure 14. The flange is modelled as two bodies, with total mass M_1, coupled by a spring with spring constant λ_1. A similar system, with total mass M_2 and spring constant λ_2, models the rod. The housing is modelled as a single mass M_3 attached to an immovable body (wall) by a spring with spring constant λ_3. The flange and the rod are attached at one end, and move toward the housing, with the flange impacting the housing as depicted in Figure 14. It is assumed that hydraulic fluid is present between the flange and the housing, and thus, a squeeze film is created during impact. As the force F_f is generated in the squeeze film, the springs associated with the piston and housing begin to compress. We also consider the forces due to the impact of the screw tip on the molten metal, which is modelled as a force acting on the leading end of the rod. The form of the force is taken without modification from the derivation

from Section 2.2. We ignore the deformation of the mold due to the pressure generated during the impact. All interactions are assumed to be elastic.

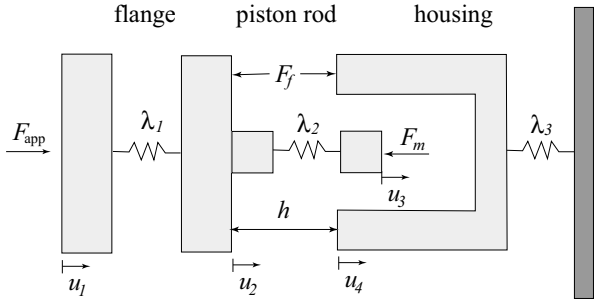

FIGURE 14: Mass-spring model for the elastic deformation of the machine parts. A cross-section is shown, where the system is assumed to be symmetric under rotation about the length-wise axis.

One of the goals of this study is to investigate the validity of the results produced by the simplified models. A comparison with a continuous version of the model, which we will consider in Section 4.2, may be able to aid in this. Thus, we will formulate the discrete model in a way that will allow direct comparisons with the more complex model.

In order to enable this comparison, we make the assumption that the two bodies of each component are each of mass kM, as shown in Figure 15, where M is the total mass, and k is a parameter that is not necessarily equal to $1/2$. The new parameter k and the spring constant λ for a general component are chosen so that solutions of the discrete model mimic those of a continuous model in some test cases that consist of applying forces on an individual component. For a detailed derivation of the equations for a single general component, including the determination of the constants k and λ, see the appendix.

The equations for a single component are separated into the motion of the centre of mass, $u_1 + u_2$, and the compression motion $u_2 - u_1$, where u_1 and u_2 are the displacements of the two masses, as depicted in Figure 15. From the appendix, we have the equations for a single

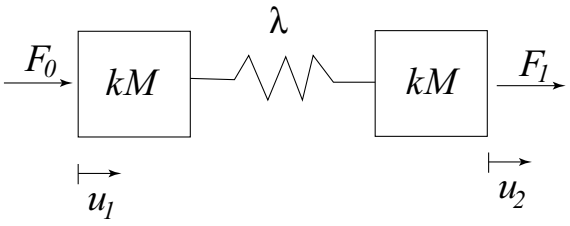

FIGURE 15: A single component of the mass-spring model. Parameters k and λ are chosen to maximize compatibility with a continuous model (see appendix). F_0 and F_1 are general forces acting on either side of the component.

component:

$$\frac{1}{2}M\left(\ddot{u}_1+\ddot{u}_2\right)=F_0+F_1, \tag{68}$$

$$\frac{2}{\pi^2}M\left(\ddot{u}_2-\ddot{u}_1\right)=F_1-F_0-2\lambda\left(u_2-u_1\right). \tag{69}$$

We use (68) and (69) to describe the motion of the piston flange, with $F_0 = F_{\text{app}}$ the applied force, and $F_1 = -F_{\text{flange}}$ the force on the flange due to contact with the piston rod. For the piston rod, we have a similar equation, but with u_1 and u_2 replaced by the appropriate displacements u_2 and u_3, respectively (as shown in Figure 14), and with $F_0 = F_{\text{rod}}$ the force on the rod due to contact with the flange, and $F_1 = -F_m$ the force due to impact with the molten metal in the mold. We consider the motion of the housing component as $1/2$ of the compression motion with total mass $2M_3$, and uncompressed spring length $2l_3$, and with $F_0 = F_f$, and $F_1 = -F_f$, where F_f is the force generated in the squeeze film given by (9).

The equations describing the displacements u_1, u_2, u_3, and u_4 for the mass-spring system shown in Figure 14 are

$$\frac{1}{2}M_1\left(\ddot{u}_1+\ddot{u}_2\right)=F_{\text{app}}-F_{\text{flange}}, \tag{70}$$

$$\frac{2}{\pi^2}M_1\left(\ddot{u}_2-\ddot{u}_1\right)=-F_{\text{flange}}-F_{\text{app}}-2\lambda_1\left(u_2-u_1\right), \tag{71}$$

$$\frac{1}{2}M_2\left(\ddot{u}_2+\ddot{u}_3\right)=F_{\text{rod}}-F_m, \tag{72}$$

$$\frac{2}{\pi^2} M_2 \left(\ddot{u}_3 - \ddot{u}_2\right) = -F_m - F_{\text{rod}} - 2\lambda_2 \left(u_3 - u_2\right), \tag{73}$$

$$\frac{4}{\pi^2} M_3 \ddot{u}_4 = F_f - \lambda_3 u_4, \tag{74}$$

where M_1, M_2 and M_3 are the total masses and λ_1, λ_2 and λ_3 are the spring constants, for the flange, the piston rod, and the machine housing, respectively, F_{app} is the applied hydraulic force, and it has been assumed that the flange and rod are always in contact, and so the displacements of the contacting ends are equal. From Section 2.2, we have that $F_m = \pi r_s^2 P_m$, where P_m can be found from the differential equation (24). The forces F_{flange} and F_{rod} are unknown, but must satisfy $F_f + F_{\text{rod}} = F_{\text{flange}}$, i.e., there must be a balance of the forces at the point of contact. The force F_f generated in the squeeze film is given only in terms of the film thickness h and its first derivative; see (9), where, in terms of the displacements, the film thickness h is given by

$$h - h(0) = u_4 - u_2. \tag{75}$$

The force F_m on the piston rod due to impact on the molten metal in the mold is given in terms the pressure P_m in the mold, which in turn is given by the differential equation (24) that depends on P_m and u_3 the displacement of the leading edge of the piston rod. In the simple model of section 2, in which the elastic deformation was ignored, the displacement of the leading edge of the piston could be chosen as the same as the film thickness. This is not the case here. To close the system we must append (24) with the variable h replaced by $h(0) - u_3$. Because only derivatives of h make significant contributions in (24), the choice of the initial constant $h(0)$ has no effect on this equation (see Section 2.2).

For the reasons described in the appendix, we take

$$\lambda_i = \frac{EA_i}{l_i}, \tag{76}$$

for $i = 1, 2, 3$ representing the flange, the piston rod and the machine housing, respectively, where E is the Young's modulus of the elastic material (assumed to be the same for all components), A_i is the cross-sectional area of the ith component, i.e., $A_1 = \pi b^2$, b is the radius of the flange, $A_2 = \pi r_s^2$, r_s is the radius of the piston rod, $A_3 = \pi(b^2 - a^2)$, b and a are the outer and inner radii of the housing, we have assumed that the radius of the flange is equal to the outer radius of the housing, and l_i is the uncompressed length of the ith component. We also take

$$M_i = \rho A_i l_i, \tag{77}$$

where ρ is the density of the elastic material, which we assume is the same for each component.

We write

$$\begin{aligned} h &= h(0) + u_4 - u_2, \\ w_1 &= u_2 - u_1, \\ w_2 &= u_3 - u_2, \end{aligned}$$

where w_1 and w_2 represent the expansion length of the flange and piston rod springs, respectively, and eliminate F_{flange}, F_{rod}, u_1, u_3, u_4 to obtain the final model equations describing the evolution of the dependent variables u_2, h, w_1, w_2:

$$(M_1 + M_2)\,\ddot{u}_2 = g(u_2, h, w_1, w_2), \tag{78}$$

$$\begin{aligned} \frac{4}{\pi^2} M_3 \ddot{h} = F_f - \lambda_3 \left(h - h(0) + u_2\right) \\ - \frac{4}{\pi^2} \frac{M_3}{M_1 + M_2} g(u_2, h, w_1, w_2), \end{aligned} \tag{79}$$

$$\left(\frac{1}{2} + \frac{2}{\pi^2}\right) M_1 \ddot{w}_1 = -2F_{\text{app}} - 2\lambda_1 w_1 + \frac{M_1}{M_1 + M_2} g(u_2, h, w_1, w_2), \tag{80}$$

$$\left(\frac{1}{2} + \frac{2}{\pi^2}\right) M_2 \ddot{w}_2 = -2F_m - 2\lambda_2 w_2 - \frac{M_2}{M_1 + M_2} g(u_2, h, w_1, w_2), \tag{81}$$

where

$$\begin{aligned} &g(u_2, h, w_1, w_2) \\ &\quad = \left(1 - \frac{\pi^2}{4}\right)(F_{\text{app}} - F_m) - \left(1 + \frac{\pi^2}{4}\right) F_f - \frac{\pi^2}{2}\left(\lambda_1 w_1 - \lambda_2 w_2\right), \end{aligned}$$

F_f is given by (9), and $F_m = A_2 P_m$, where the differential equation (24) for P_m, with dh/dt replaced by $\dot{u}_3 = \dot{w}_2 + \dot{u}_2$, must be added to complete the system.

As in Section 2, we carry out some numerical calculations. An example in which it is assumed that the mold force is zero is plotted in Figure 16. We take the Young's modulus $E = 2 \times 10^{11}$, the density of the elastic material $\rho = 8 \times 10^3 \text{kg/m}^3$, and the uncompressed lengths of the bodies to be $l_1 = 0.3\text{m}$, $l_2 = 1\text{m}$, and $l_3 = 1.3\text{m}$, for the flange, rod

and housing, respectively. All other relevant parameters are taken to be those in Table 1. Initially, the housing is stationary and the springs of the flange and piston rod are not compressed. As the piston approaches the housing, the effects of the squeeze film begin to be felt and the spring of the flange begins to be compressed, while the spring of the piston rod is expanded. As the flange impacts the housing, the squeeze film pressure spikes, with corresponding increases in the rates of change of the squeeze film height. After impact, the squeeze film pressure decays, and the height of the squeeze film approaches zero at a slower rate than initially. Of particular interest is that the maximum force that is observed in the squeeze film is approximately 2.5×10^6N, while in the situation where the elasticity of the machine parts is not considered, the maximum force is more than 8×10^6N. That is, in this case, the elasticity of the machine parts acts to reduce the impact force by more than three times.

4.2 A continuous model with elastic deformation In this section, we consider a simple one dimensional model in which the flange, piston and housing are all assumed to be one dimensional elastic bodies in which elastic vibrations are governed by the one dimensional elastic wave equation

$$\rho \frac{\partial^2 u}{\partial t^2} = E \frac{\partial^2 u}{\partial x^2} \,,$$

where $u = u(x,t)$ is the displacement, which is a function of position x within the body and time t, ρ is the density, and E is the Young's Modulus of the material. See, e.g., Love [**19**].

The flange and the piston are considered as two distinct bodies for which the displacement is continuous at the interface, but the stress is discontinuous owing to the force provided by the squeeze film (see Figure 17). The housing is considered as one body. The displacements for the flange, the piston rod, and the housing are taken to be $u_i = u_i(x,t),\ i = 1,2,3$, respectively, with corresponding uncompressed lengths l_i. As in the discrete model, the cross-sectional areas of the three bodies are $A_1 = \pi b^2$ for the flange, $A_2 = \pi r_s^2$ for the piston, and $A_3 = \pi(b^2 - a^2)$ for the housing, where it is assumed that all bodies are symmetric under rotation about the length-wise axis. For simplicity we assume the same Young's Modulus E and density ρ for all three bodies. The elastic wave speed in the bodies is given by $c = \sqrt{E/\rho}$. We also assume an initial velocity v_{init} for the flange and piston, and an applied force F_{app} at the end of the flange.

The position x in the flange and piston is measured in the direction

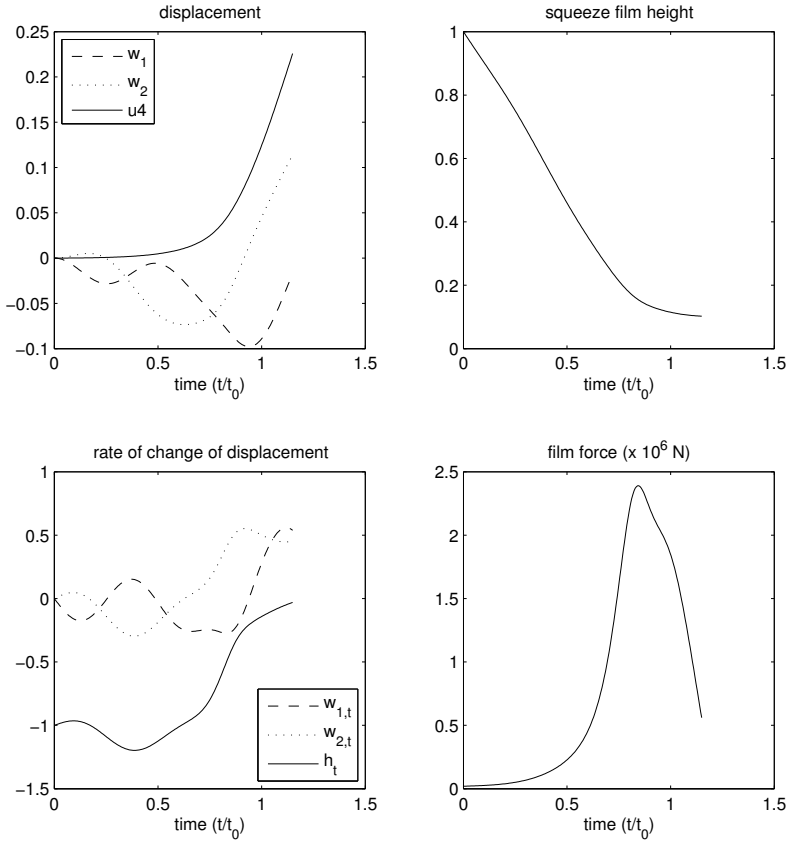

FIGURE 16: Results from the mass-spring model, which includes both the effects of the squeeze film and the effects of the elasticity of the machine parts. The displacements w_1, w_2 and u_4 represent the compression of the springs for the flange, piston rod, and housing, respectively; a negative displacement represents a compression of the spring. The displacements and squeeze film height have been scaled by h_0, and time has been scaled by t_0.

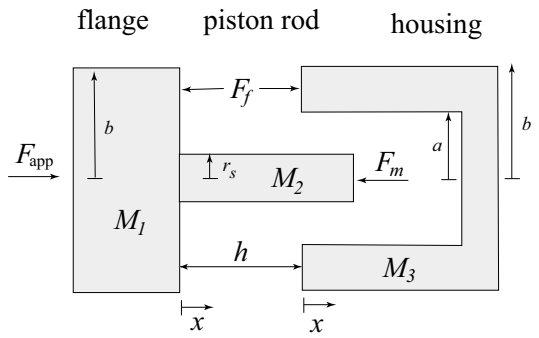

FIGURE 17: The continuous one-dimensional model of the elastic deformation of the machine parts. A cross-section is shown, where the system is assumed to be symmetric under rotation about the length-wise axis.

of motion of the two bodies with $x = 0$ being taken as the interface, as indicated in Figure 17; thus $u_1(x,t)$ is defined on $x \in [-l_1, 0]$, and $u_2(x,t)$ is defined on $x \in [0, l_2]$. The position x for the housing is in the same direction but is measured from the initial position of the housing; thus, $u_3(x,t)$ is defined on $x \in [0, l_3]$. We will assume that the housing is fixed at its non-interacting end $x = l_3$.

The motion of the three bodies will be driven by the applied force F_{app}, the force F_f in the squeeze film, and the force F_m in the mold. These forces will be governed by the same equations that appear in Section 2.

We use the Laplace transform in t, and find that the transforms $\widehat{u_i} = \widehat{u_i}(x,s)$ of the displacements u_i can be written as

$$\widehat{u_1} = \frac{v_{\text{init}}}{s^2} + a_1 \exp(sx/c) + b_2 \exp(-sx/c), \tag{82}$$

$$\widehat{u_2} = \frac{v_{\text{init}}}{s^2} + a_2 \exp(sx/c) + b_2 \exp(-sx/c), \tag{83}$$

$$\widehat{u_3} = a_3 \exp(sx/c) + b_3 \exp(-sx/c), \tag{84}$$

where it has been assumed that the initial values for u_i are all zero, and $\partial u_{1,2}/\partial t = v_{\text{init}}$ and $\partial u_3/\partial t = 0$ at $t = 0$. The boundary conditions for the transforms $\widehat{u_i}$ are

$$EA_1 \frac{\partial \widehat{u_1}}{\partial x} = -\widehat{F_{\text{app}}} \quad \text{at } x = -l_1, \qquad \widehat{u_1} = \widehat{u_2} \quad \text{at } x = 0, \tag{85}$$

for the flange,

$$
\begin{aligned}
EA_1\frac{\partial \widehat{u}_1}{\partial x} &= EA_2\frac{\partial \widehat{u}_2}{\partial x} - \widehat{F_f} \quad \text{at } x = 0,\\
EA_2\frac{\partial \widehat{u}_2}{\partial x} &= -\widehat{F_m} \qquad\qquad\quad \text{at } x = l_2,
\end{aligned}
\tag{86}
$$

for the piston rod, and

$$
EA_3\frac{\partial \widehat{u}_3}{\partial x} = -\widehat{F_f} \quad \text{at } x = 0, \qquad \widehat{u_3} = 0 \quad \text{at } x = l_3, \tag{87}
$$

for the housing.

To close the system one must note that F_m is related to $u_2(l_2, t)$ via the differential equation (24) (with h of that equation replaced by $u_2(l_2, t)$), F_f is given in terms of the squeeze film thickness h which is itself given by,

$$
h = h(0) + u_3(0, t) - u_1(0, t). \tag{88}
$$

These six boundary conditions enable us to determine the six constants a_i, b_i of (82)–(84) in terms of the transforms of h, F_m and F_f. Then, the equations for the transforms $\widehat{u}_i$, together with appropriate initial conditions, allow us to determine h, F_m and F_f.

A complete solution is not difficult but involves a substantial amount of book keeping as one has to keep track of various discontinuous forces arising from the reflections of elastic waves. We therefore give an indication of how the solution may be derived followed by some actual solutions where the elapsed time is limited to exclude most of the reflections but is long enough to give some idea of the solution.

We substitute the transform $\widehat{u_3}$ given by (84) into the boundary conditions (87) and obtain

$$
a_3 \exp(sl_3/c) + b_3 \exp(-sl_3/c) = 0, \tag{89}
$$

$$
EA_3(a_3 \exp(sl_3/c) - b_3 \exp(-sl_3/c)) = -c\widehat{F_f}/s. \tag{90}
$$

These equations can be solved to find a_3, b_3, and hence the transform $\widehat{u_3}$. Because we will only need the value of u_3 at $x = 0$ to find h and F_f, we write

$$
\widehat{u_3}(0, s) = \frac{c\widehat{F_f}}{EA_3 s}\left(\frac{1 - \exp(-2sl_3/c)}{1 + \exp(-2sl_3/c)}\right).
$$

We formally expand the denominator in powers of $\exp(-2sl_3/c)$, note that the inverse transform of $e^{-\alpha s}/s$ is the Heaviside function $H(t-\alpha)$, and use the convolution theorem to obtain

$$u_3(0,t) = \frac{c}{EA_3}\int_0^t F_f(\tau)\left(1 + 2\sum_{j=1}^{\infty}(-1)^j H(t-\tau-2jl_3/c)\right)d\tau,$$

where the Heaviside functions represent reflections from the fixed end of the housing. Expressions for $u_1(0,t)$ and $u_2(l_2,t)$ in terms of F_m and F_f can be found in a similar manner.

We now look for solutions for the forces F_f and F_m limited in time to three reflections at the squeeze film and one at the mold. We do not give the details but again denominators may be expanded in powers of exponentials which, upon inverse transformation, lead to Heaviside functions representing multiple reflections from the ends of both the flange and the piston. We write $T_i = l_i/ct_0$ for the scaled reflection times and limit our solution to a scaled time of less than $4T_1$. With a choice of the uncompressed body lengths $l_1 = 0.3$, $l_2 = 1$ and $l_3 = 1.5$, the only reflections that are retained are up to $3T_1$ and $T_1 + T_2$.

The equations above together with the differential equation (24) for P_m and the equation $F_f = -6\mu I h_t/h^3$ lead to the following results for h, F_f, and F_m where h is the height of the squeeze film scaled by h_0, and time t and the wave speed c have been scaled by t_0.

$$\begin{aligned}(91)\qquad \Gamma\left(\frac{1}{h^2(t)} - \frac{1}{h^2(0)}\right) &= t + h(t) - h(0)\\ &+ \frac{2\alpha_1 F_{\text{app}} c}{(1-\alpha_3)EA_1h_0}(t-T_1)H(t-T_1)\\ &- \frac{2\alpha_1\alpha_3}{(1-\alpha_{3)}}\left[t - 2T_1 + h(t-2T_1) - h(0)\right]H(t-2T_1)\\ &\frac{2\alpha_1 F_{\text{app}} c(2\alpha_1-1)}{(1-\alpha_3)E(A_1+A_2)h_0}(t-3T_1)H(t-3T_1)\\ &- \frac{2cH(t-T_2)}{E(A_1+A_2)(1-\alpha_3)h_0}\int_0^{t-T_2} F_m(\tau)d\tau,\end{aligned}$$

$$
\begin{aligned}
(92)\qquad F_f = \frac{2\Gamma}{2\Gamma + h^3(t)}\Bigg[& \frac{EA_3h_0}{c}(1-\alpha_3) \\
& + 2\alpha_3 F_{\text{app}} H(t-T_1) - \frac{2\alpha_1\alpha_3 F_f(t-2T_1)}{(1-\alpha_3)} H(t-2T_1) \\
& + \frac{2\alpha_3 F_{\text{app}} c(2\alpha_1+\alpha_3-1)}{(1-\alpha_3)} H(t-3T_1) \\
& - 2\alpha_3 F_m(t-T_2)H(t-T_2)\Bigg],
\end{aligned}
$$

$$
\begin{aligned}
(93)\qquad F_m = {} & \frac{A_2^2 h_0}{\varepsilon V_0 B}\left[1-\exp(-Bt)\right] \\
& - \frac{2A_2^2 cH(t-T_2)}{\varepsilon V_0 E(A_1+A_2)} \int_0^{t-T_2} F_f(\tau)\exp\left(-B(t-T_2-\tau)\right)\, d\tau \\
& + \frac{4\alpha_1(2-\alpha_3)A_2^2 cF_{\text{app}}}{\varepsilon V_0 EA_1(1-\alpha_3)B}\left[1-\exp\left(-B(t-T_1-T_2)\right)\right] \\
& \times H(t-T_1-T_2),
\end{aligned}
$$

where

$$
\Gamma = \frac{3\mu Ic}{EA_3h_0^3t_0(1-\alpha_3)}, \quad \alpha_i = \frac{A_i}{A_1+A_2+A_3}, \quad B = \gamma + \frac{A_2c}{\epsilon EV_0},
$$

and γ is the leakage ratio given in (35).

These formulae are used to find the scaled gap width h, and the forces acting in the squeeze film F_f and the force in the mold F_m using the same parameter values as in the previous section. In addition to the above models, we also make comparisons with a hybrid model, which consists of computing the film thickness h from the discrete model, then substituting this (approximate) function into the formula that is derived from the continuous model (92).

In Figure 18, an example is shown in which the mold force is neglected and the parameters are taken to be the same as those in the example in Section 4.1, with the exception of the initial value of h which is taken to be $h(0) = 0.5$. The forces calculated in the mass-spring model and in the continuous model are initially very close. Eventually, they begin to diverge, with the force in the mass-spring model growing to its maximum value more quickly. Once it reaches its maximum value, there is a single oscillation before it begins to decay. The force in the continuous

model increases more slowly, and is not as smooth, owing to the explicit consideration of the reflections of the elastic waves at the boundaries of the bodies. The force then begins to decay without an observed large amplitude oscillation. There are two very interesting observations. The first is that the maximum force in the mass-spring model is very similar to that predicted in the continuous model. The second is that the sharp changes that are observed in the continuous model seem to be commensurate with the oscillations in the mass-spring model. That is, the mass-spring model is able to reproduce two important features of the elastic deformation of the continuous model, although it is significantly easier to implement, or to extend to include other effects that have not been consider (see, e.g., the next section).

The growth of the force calculated in the hybrid model more closely follows the force of the continuous model. In general, with the exception of a large jump at small time, the force profile of the hybrid model is similar to that of the continuous model. However, the maximum force is slightly higher by approximately 15%. The hybrid model is also much more easily extended than the continuous model, as seen in the next section.

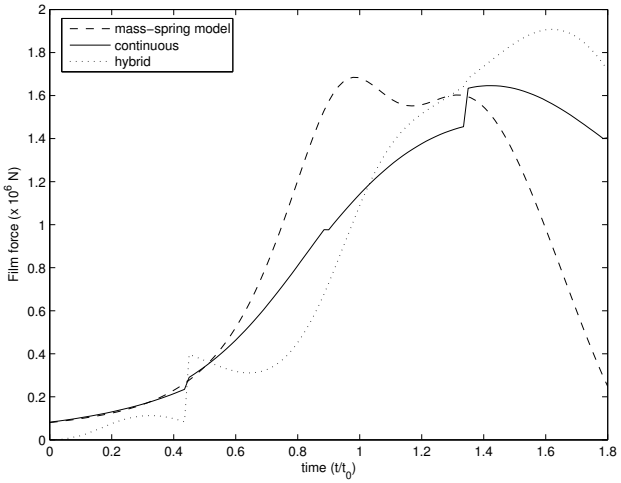

FIGURE 18: Comparison of dimensional film force in mass-spring, continuous and hybrid models. Time has been scaled by t_0.

5 Variable viscosity via the Barus law Given the forces that are predicted to occur in the squeeze film, it is possible that the viscosity and density of the hydraulic fluid may vary. For a detailed discussion of such effects, see for example, Gohar [**10**] and Dowson and Higginson [**8**].

The effect of pressure p on viscosity μ (at constant temperature) can be described by the Barus law

$$\mu = \mu_0 \exp(\alpha p), \tag{94}$$

where μ_0 is the viscosity at zero pressure, and α is an empirical constant called the pressure viscosity coefficient. For a typical heavy mineral oil, such as the hydraulic fluid, $\alpha \sim 25 \times 10^{-9}$ m^2/N. In very high pressure contacts the fluid can attain a 'glass transition' where it starts to behave like a solid.

Density variations are typically less significant than viscosity variations. For a mineral oil, a standard relation that gives the variation of the density ρ with pressure p is

$$\rho = \rho_0 \left(1 + \frac{6 \times 10^{-10} p}{1 + 1.7 \times 10^{-9} p}\right), \tag{95}$$

where ρ_0 is the density at zero pressure.

If we consider the expressions (94) and (95) in the present context, we find that the density variation of the hydraulic fluid may be of the order 10%, while its viscosity may increase by a factor of over 1000 in a small region where the pressure reaches its maximum. Thus, it is quite possible that this variation in viscosity could significantly effect the forces that are predicted. For this reason we will now modify the model to incorporate the effect of viscosity variation via the Barus law.

We return to the reduced Navier-Stokes equations (2)–(4), which model the flow of the hydraulic fluid between the piston flange and housing as a squeeze film, but now we allow the viscosity to vary according to the Barus law (94). Equation (3) indicates that $p = p(r, t)$, which via the Barus law indicates that $\mu = \mu(r, t)$. The model development follows through the same steps as in Section 2.1 until equation (7). At this stage we change $\mu_0 \to \mu_0 \exp(\alpha p)$ to find

$$e^{-\alpha p} \frac{\partial p}{\partial r} = \frac{6\mu_0}{h^3} \frac{dh}{dt} \left(r - \frac{b^2}{r}\right). \tag{96}$$

Integrating once more and applying $p(a,t) = P_a$ leads to

$$p = P_a - \frac{1}{\alpha}\log\left[1 - \frac{6\alpha\mu_0}{h^3}\frac{dh}{dt}\left(\frac{r^2-a^2}{2} - b^2\log\frac{r}{a}\right)e^{\alpha P_a}\right]. \tag{97}$$

In the limit $\alpha \to 0$, we retrieve the previous expression for pressure. The expression (97) indicates that as the quantity inside the square brackets approaches zero, the pressure, and therefore the viscosity, will grow without bound. Thus, it is expected that as the quantity $1/h^3\ dh/dt$ becomes large, the quantity inside the square bracket will become small, causing the viscosity to grow. This in turn will cause the piston to decelerate more quickly, i.e., dh/dt will decrease quickly, which will prevent the pressure from going to infinity.

The force F_f in the squeeze film can be found by evaluating

$$F_f = 2\pi\int_a^b pr\,dr. \tag{98}$$

In general, this integral must be approximated numerical. However, this does not pose a problem in the implementation into the mass-spring (and thus the hybrid model). In particular, for the numerical approximation of the solutions in the mass-spring model, the integral (98) must be calculated at each time step. In Figure 19 typical results are shown for the film height, and its rate of change, and the film force, for the mass-spring model with the effects of the variation of viscosity both included and ignored. The relevant parameter values are chosen as in Section 4.2, and $\alpha = 25 \times 10^{-9}\text{m}^2/\text{N}$. In Figure 19(a) it can be clearly seen that the increased viscosity leads to film heights significantly larger than those obtained with an isoviscous model. The rate of change of the film height h is effectively primarily at intermediate time, with the variable viscosity model exhibiting a sharper decrease. Figure 19(c) shows the corresponding force profiles. The force is highest in the variable viscosity model in which it reaches a value of approximately $2.2 \times 10^6\text{N}$, which is approximately 25% higher than that predicted in the isoviscous model. The values of these forces lead to pressures well below the upper bound set for the applicability of the Barus pressure viscosity law (94).

Similar results are shown for the force calculated from the hybrid model. As discussed above, it is very difficult to find solutions of the continuous model when the viscosity is allowed to vary. However, for the hybrid model this does not pose a problem. Interestingly, the calculated forces for the variable viscosity and isoviscous cases are very similar. Indeed, the force in the isoviscous model is slightly larger of the two.

In Figure 21 the viscosity variation, according to the Barus law, is shown. The viscosity at zero pressure is $\mu_0 = 0.01\text{Ns/m}^2$, while the maximum viscosity predicted by the model is approximately 50Ns/m^2, i.e., the maximum viscosity is nearly 5000 times the ambient viscosity.

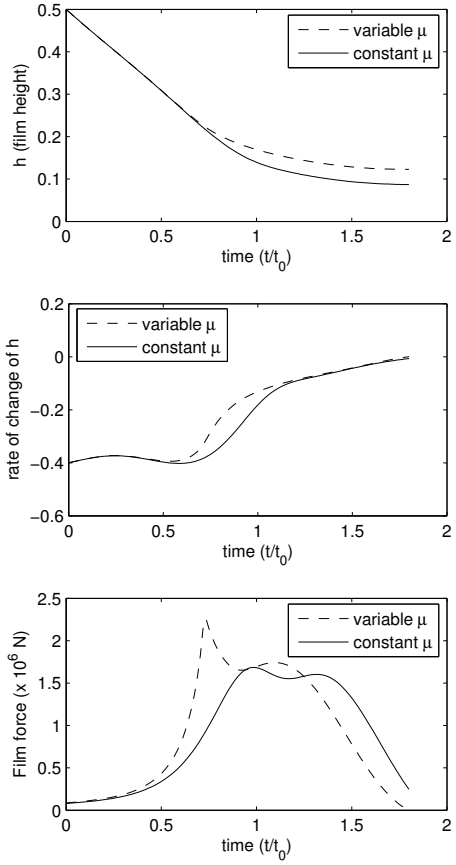

FIGURE 19: Comparison of isoviscous and Barus law cases for results computed in the mass-spring model. The film height h, rate of change of film height dh/dt, and dimensional film force F_f for the two cases are compared. The squeeze film height h has been scaled by h_0, and time has been scaled by t_0.

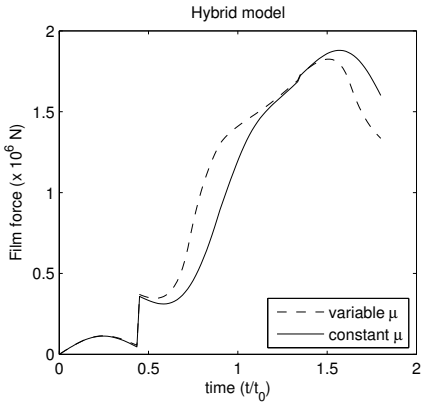

FIGURE 20: Comparison of isoviscous and Barus law cases for the film force computed in the hybrid model.

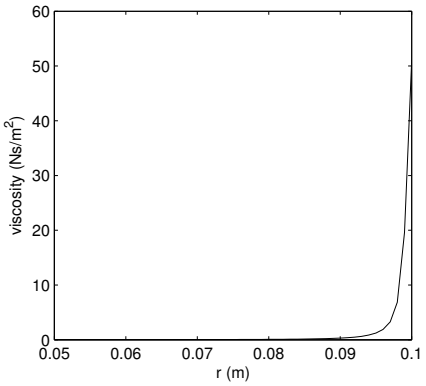

FIGURE 21: Variation of the viscosity with the radial coordinate r at the time in the cycle when the maximum pressure is attained. The viscosity is computed from the Barus law.

6 Concluding remarks There are many parameters involved in the injection molding of a product. Much of the literature focuses on adjusting the parameters to maximize product quality and minimize cost. For example, much cost benefit can result if a molding material can be developed that has lower raw material costs, or that reduces energy

consumption (e.g., has lower melt temperature), or that leads to reduced product defects, in particular under increases in cycle time. However, any change in these parameters has the potential of leading to a reduced life-time for the injection molding machine, which can greatly outweigh any cost gains obtained by the increase in efficiency of production. The models developed here can be used to predict how the impact forces, that occur during a production cycle, will vary as parameters are varied. The predicted forces can then be used to assess whether the machine has been adequately designed.

We present a series of models that include effects due to the presence of hydraulic fluid between the piston flange and piston rod, the variation of the viscosity of this fluid with pressure, the elasticity of the machine parts and molten metal, and the leakage of molten metal past the screw tip, which all can produce significant effects on the pressure profiles. In cases in which the piston decelerates primarily due to impact with the molten metal in the mold (i.e., due to the mold force), the impact forces are generally smaller than in cases in which the deceleration occurs primarily due to impact of the piston flange on the housing (i.e., due to the film force). It is found that the predicted film force may be more than 3 times greater in the model that neglects the elasticity of the machine parts, and the mass-spring model with variable viscosity predicts film forces approximately 25% greater than in the mass-spring model that neglects this effect.

While the first model that is developed ignores the elasticity of the machine parts, its simplicity is amenable to analytical analysis. It is expected that this model would be effective for the investigation of qualitative effects of changes in the parameters. The mass-spring model of Section 4.1 is the simplest system that takes into account the elasticity of the machine parts. Even so, solutions of the model are similar to those found in the more realistic continuous one-dimensional model, as well as a hybrid model, both of which are discussed in Section 4.2. Furthermore, solutions of the mass-spring model are easily computed, and it is straightforward to extend this model as seen in Section 5 where the viscosity of the hydraulic fluid is considered to vary according to the Barus law. This is not the case for the continuous model, while the hybrid model may be easily extended in some cases. The extendibility is a very important feature of a model because it is expected that a company may wish to include a variety of other factors that were not considered here.

7 Appendix: derivation of the discrete model with elasticity In this appendix, we derive the equations of motion for a general single mass-spring component. We make the assumption that the two bodies of each component are each of mass kM, as shown in Figure 22, where M is the total mass, and k is a parameter that is not necessarily equal to $1/2$. The new parameter k and the spring constant λ for a general component are chosen so that solutions of the discrete model mimic those of a continuous model in some test cases that consist of applying forces on an individual component.

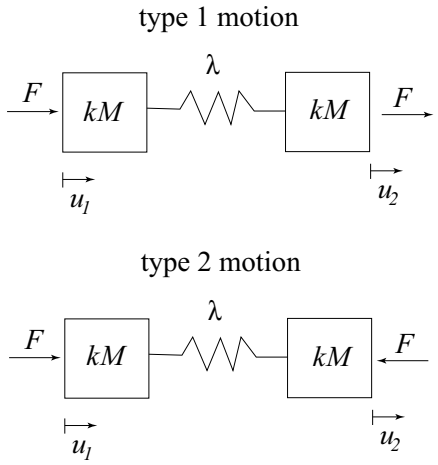

FIGURE 22: Two different types of motion used to formulate the mass-spring model in a way that it is compatible with the continuous model.

It is necessary to consider two kinds of motion: (1) motion of the centre of mass, and (2) motion due to compression of the spring. See Figure 22. In the centre of mass motion, a force F is applied to each of the two masses. In this case, we expect the centre of mass to satisfy

$$M\left[\frac{1}{2}\left(\ddot{u}_1+\ddot{u}_2\right)\right]=2F, \tag{99}$$

where u_1 and u_2 are the displacements for the two masses, M is the total mass, F is the force, and a dot represents a derivative with respect to time t. With initial conditions, $u_1(0)=u_2(0)=0$, $\dot{u}_1(0)=\dot{u}_2(0)=v_{\text{init}}$,

where v_{init} is some constant, we also expect $u_1 = u_2$ for all time, i.e., the spring does not become compressed or extended. If we write down the equations of motion for the discrete component for this "type 1" motion, pictured at the top of Figure 22, we obtain

$$\begin{aligned} kM\ddot{u}_1 &= F + \lambda(u_2 - u_1), \\ kM\ddot{u}_2 &= F - \lambda(u_2 - u_1). \end{aligned} \tag{100}$$

Adding the two equations we obtain

$$kM(\ddot{u}_1 + \ddot{u}_2) = 2F. \tag{101}$$

Therefore, for the model to correspond to (99), we should choose our parameter $k = 1/2$.

For the second kind of motion, we choose our test case to be a situation where a force F is applied to one of the masses, while a force of $-F$ is applied to the other. This "type 2" motion is shown at the bottom of Figure 22. In this case, the equations describing the displacement of the two masses of the discrete component are

$$\begin{aligned} kM\ddot{u}_1 &= F + \lambda(u_2 - u_1), \\ kM\ddot{u}_2 &= -F - \lambda(u_2 - u_1). \end{aligned} \tag{102}$$

Subtracting the first equation from the second, we obtain

$$kM(\ddot{u}_2 - \ddot{u}_1) = -2F - 2\lambda(u_2 - u_1). \tag{103}$$

With reasonable initial conditions, we expect $u_2 = -u_1$ for all time. With initial conditions chosen as $u_2 - u_1 = \dot{u}_2 - \dot{u}_1 = 0$ at $t = 0$, the solution is

$$u_2 - u_1 = -\frac{F}{\lambda}(1 - \cos\omega t), \tag{104}$$

where $\omega^2 = 2\lambda/kM$, with $u_2 = -u_1$. Thus,

$$u_1 = \frac{F}{2\lambda}(1 - \cos\omega t). \tag{105}$$

If the same initial conditions are applied in a simple one-dimensional continuous model for elastic deformation of a body with Young's modulus E, uncompressed length l, cross-sectional area A (assumed constant),

and density ρ, the displacement at $x = 0$ (corresponding to u_1 of the discrete component) is

$$u(x=0,t) = \frac{cF}{EA}\left[t - 2\left(t - \frac{l}{c}\right)H\left(t - \frac{l}{c}\right) + 2\left(t - \frac{2l}{c}\right)H\left(t - \frac{2l}{c}\right) + \dots\right], \tag{106}$$

where $c = \sqrt{E/\rho}$ is the elastic wave speed, and $H(t-\alpha)$ is the Heaviside function with delay α, i.e., $H(t-\alpha) = 0$ for $t < \alpha$, and $H(t-\alpha) = 1$ for $t > \alpha$. See Section 4.2 for a more detailed description of continuous elastic deformation. A plot of (106) would reveal a saw-tooth shaped graph, with linear growth over a time l/c from zero to Fl/EA, followed by linear decay from Fl/EA to zero over the same interval, i.e., the graph is continuous with discontinuous first derivative at intervals of l/c. Thus, the period of oscillation is $2l/c$ and the maximum deformation is Fl/EA.

To ensure that the maximum of the deformations for the discrete (105) and continuous (106) models are equal, we can choose

$$\lambda = \frac{EA}{l}\,, \tag{107}$$

which is very reasonable. The period in the continuous model is $2l/c$. In order for the period ω for the solution of the discrete model to match this, we require

$$\frac{2\pi}{\omega} = \frac{2l}{c}\,,$$

and thus,

$$\omega^2 = \frac{\pi^2 c^2}{l^2} = \frac{2\lambda}{kM} = \frac{2EA}{kMl}\,. \tag{108}$$

This suggests that we choose

$$k = \frac{2EAl}{\pi^2 M c^2}\,. \tag{109}$$

Because $M = \rho Al$ and $E = \rho c^2$, this becomes

$$k = \frac{2}{\pi^2}\,. \tag{110}$$

For a general situation, where a force F_0 is applied to one side of the discrete component and a force F_1 is applied to the other, as shown in Figure 15, we separate into two cases, each similar to one of the two motions described above. That is, we write down one equation for u_1+u_2 describing the centre of mass motion, where the force $F = F^+ = (F_0 + F_1)/2$, and use $k = 1/2$ in this equation. Then we write down another equation for $u_2 - u_1$ describing the compression motion, where the force $F = F^- = (F_0 - F_1)/2$, and use $k = 2/\pi^2$. The equations for a single component become

$$\frac{1}{2}M\left(\ddot{u}_1 + \ddot{u}_2\right) = 2F^+ = F_0 + F_1, \tag{111}$$

$$\begin{aligned}\frac{2}{\pi^2}M\left(\ddot{u}_2 - \ddot{u}_1\right) &= -2F^- - 2\lambda\left(u_2 - u_1\right) \\ &= F_1 - F_0 - 2\lambda\left(u_2 - u_1\right),\end{aligned} \tag{112}$$

which we use to describe the motion of the piston flange and piston rod, with F_0 and F_1 replaced by the respective forces on the component; see Section 4.1. The motion of the housing component is considered as $1/2$ of the compression motion with total mass $2M_3$, and uncompressed spring length $2l_3$.

REFERENCES

1. P. J. Blau and M. Walukas, *Sliding friction and wear of magnesium alloy az91d produced by two different methods* Tribology International **33** (2000), 573–579.
2. D. M. Bryce, *Plastic Injection Molding... manufacturing process fundamentals*, Society of Manufacturing Engineers, Dearborn, Michigan, 1996.
3. M. Bulger, *Metal injection molding*, Advanced Materials and Processes **1**(1) (2005), 39–40.
4. F. Czerwinski, *The microstructural development of Mg-9 Pct Al-1 Pct Zn alloy during injection molding*, Metallurgical and Materials Transactions **33A**(9) (2002), 2963–2972.
5. F. Czerwinski, *Magnesium alloy particulates for thixomolding applications manufactured by rapid solidification*, Material Science and Engineering, A **367** (2004), 261–271.
6. Y.-M. Deng, Y. C. Lam, S. B. Tor and G. A. Britton, *A CAD-CAE integrated injection molding design system*, Engineering with Computers **18** (2002), 80–92.
7. C. Diduch, R. Dubay and W. Gui Li, *Temperature control of injection molding. Part I: Modeling and identification*, Polymer Engineering and Science **44**(12) (2004), 2308–2317.

8. D. Dowson and G. R. Higginson, *Elastohydrodynamic Lubrication*, Pergammon Press, Oxford, U.K., 1977.
9. J. L. Garcia, K. W. Koelling and J. W. Summers, *Computational prediction of pvc degradation during injection molding in a rectangular channel*, Polymer Engineering and Science **44**(7) (2004), 1295–1312.
10. R. Gohar, *Elastohydrodynamics*, Imperial College Press, London, U.K., 2001.
11. C. A. Hieber, V. W. Wang and K. K. Wang, *C-flow: A CAE package with high-level interactive graphics*, in *Applications of Computer Aided Engineering in Injection Molding* (L. T. Manzione, ed.), Hanser Publishers, 1987, 230–246.
12. D. Jobb. *Making complex shapes of metal*, Nickel Magazine **16**(4), 2001.
13. L. Kong, J. Y. H. Fuh, K. S. Lee, X. L. Liu, L. S. Ling, Y. F. Zhang and A. Y. C. Nee. *A Windows-native 3D plastic injection mold design system*, Journal of Materials Processing Technology, **139** (2003), 81–89.
14. H. C. W. Lau, C. K. M. Lee, W. H. Ip, F. T. S. Chan and R. W. K. Lueng, *Design and implementation of a process optimizer: a case study on monitoring molding operations*, Expert Systems **22**(1) (2005), 12–21.
15. Y. B. Lee and T. H. Kwon, *Modeling and numerical simulation of residual stresses and birefringence in injection molded center-gated disks*, Jour. of Materials Processing Technology **111** (2001), 214–218.
16. G. M. Lewis, *The effects of impact on design features*, in Proceedings of the 8th PIMS-MITACS Industrial Problem Solving Workshop (C. S. Bohun, ed.), 2004, 37–51.
17. J.-Z. Liang, *An optimal design of cooling system for injection mold*, Polymer Plastic Technology and Engineering **41**(2) (2002), 261–271.
18. Z.-C. Lin and M.-H. Chou, *Design of the cooling channels in nonrectangular plastic flat injection mold*, Jour. of Manufacturing Systems **21**(3) (2002), 167–186.
19. A. E. H. Love, *A Treatise on the Mathematical Theory of Elasticity*, 3rd ed., Cambridge University Press, Cambridge, U.K., 1977.
20. F. Shi, Z. L. Lou, J. G. Lu and Y. Q. Zhang, *Optimisation of plastic injection moulding process with soft computing*, Advanced Manufacturing Technology **21** (2003), 656–661.

Corresponding Author:

Gregory Lewis

Faculty of Science, University of Ontario IT, Oshawa. ON

E-mail address: